

# FAST PLASMA PROCESSES IN ACTIVE GALACTIC NUCLEI

V. KRISHAN

*Indian Institute of Astrophysics, Bangalore 560 034, India*

(Received 10 December, 1996)

**Abstract.** The physics of active galactic nuclei (AGN) and related objects is one of the most actively pursued areas in astrophysics. Their large luminosities over the entire electromagnetic spectrum combined with extremely short-time variability has stimulated a large number of astrophysicists to propose rather unconventional ideas. After a simplistic review of the early work on AGN, a case is made for the important role of some of the nonlinear plasma processes in the generation of the nonthermal continuum as well as its interaction with the plasma surrounding the central source in the form of accretion disks and emission line regions. These plasma processes are fast, as they operate on characteristic time scales much shorter than the single particle processes do. Due to their collective nature, the efficiencies of scattering, absorption and emission increase many fold. In particular, it is shown how the parametric instabilities cause anomalous absorption and scattering and in turn heat the plasma to much higher temperatures than could be achieved through particle collisions. A combination of the stimulated Raman and Compton scattering processes is shown to be able to account for the major part of the spectrum of 3C273, as an example. An attempt is made to address simultaneously the questions of acceleration of particles and their radiation through the concerted action of a sequence of plasma processes. This review ends with some reflections on future research directions.

## Table of Contents

1. Introduction
2. Continuum Emission of Active Galactic Nuclei
3. Early Models of Continuum Emission
4. Plasma Processes
  - 4.1. Plasma-Radiation Coupling
  - 4.2. The Instability Mechanism
    - 4.2.1. The Ponderomotive Force
    - 4.2.2. Dispersion Relation
5. The Parametric Decay Instability in Quasars
  - 5.1. Incoherence of the Incident Field
  - 5.2. Heating of Emission Line Regions
  - 5.3. 21-cm Absorption
  - 5.4. Variants of PDI
6. Stimulated Raman and Compton Scattering in Quasars
  - 6.1. Heating of the Intercloud Medium
  - 6.2. Reprocessing of the Synchrotron Self-Absorbed Radiation
  - 6.3. Polarization Variability
  - 6.4. Superluminal Motion
7. Plasma Mechanisms for Variability
8. Nonthermal Continuum
  - 8.1. Energetic Electrons
  - 8.2. The Scattering Agency
  - 8.3. Production of Radiation
9. Reflections

## 1. Introduction

Quasars are the most distant and the most luminous objects in the Universe. The optical spectra of quasars consist of strong and broad emission lines, some of which have been identified to be the Balmer series of the hydrogen spectrum, shifted to longer wavelengths. The amount of shift implies that many of these objects are moving away at a large fraction of the speed ( $c$ ) of light. If this is a cosmological red shift then one finds using the Hubble law of the expansion of the Universe that these objects are at the farthest reaches of the Universe. Quasars radiate almost over the entire electromagnetic spectrum with a typical power of  $\sim 10^{46-47}$  erg s $^{-1}$ . The Sun, for example emits  $\simeq 3.9 \times 10^{33}$  erg s $^{-1}$ . A typical galaxy has about  $10^{11}$  stars in it. Thus the output of a quasar is much more than that of an entire galaxy. However, on optical images, it appears more like a star. Here lies the origin of the name quasi-stellar objects. Further, the observed rapid time ( $t_v$ ) variability of the radiation constrains the size ( $d$ ) of the source to be extremely small ( $d < ct_v$ , if internal relativistic motions are ignored) typically of the order of  $\gtrsim 10^{14}-10^{15}$  cm, comparable to the size of the solar system (e.g., Mushotzky et al., 1993).

What could be the nature of this ‘little big’ powerhouse? We know that the stars shine due to the thermonuclear burning of hydrogen and other elements. We are also aware of the efficiency ( $\sim 0.007$ ) with which mass is converted into radiation in a thermonuclear reaction. It was concluded that quasars need a mechanism more efficient than thermonuclear burning. The consensus at present is that the energy extracted from the gravitational infall of gas on to a compact object like a black hole (Rees, 1977), fits the bill. It is akin to terrestrial hydroelectric power generation! Thus, a viable model of a quasar consists of a massive black hole accreting gas from its neighbourhood (the reservoir!). The gas, as it spirals in and accelerates becomes hot and emits photons through a variety of radiation processes. The luminosity  $L$  may be related to the mass accretion rate  $\dot{M}$  as  $L = \eta \dot{M} c^2$ , where  $\eta$ , an efficiency factor, is determined from the nature of the accretion. It is of the order of 0.3 for disc accretion onto a rapidly rotating blackhole (Novikov and Thorne, 1973), where the accreting gas has angular momentum and therefore settles down in the form of a disk around the massive central object.

The mass of the black hole can be estimated from several considerations. For example, one could demand that the gravitational attraction of the accreting gas by the black hole is larger than its repulsion by the radiation emitted. This defines the well-known Eddington limit  $L_E$  and can be derived as forces due to gravitation and radiation are different for electrons and protons, as a result of which charge separation takes place and an electric field  $E$  is set up, the system, then tries to attain an equilibrium in which the electrons and protons experience equal forces and they move together and the luminosity at which this happens is given by  $L_E = 4\pi GMm_p c / \sigma_T$ , where  $G$  is the gravitational constant,  $M$  the mass of the black hole,  $m_p$  the mass of a proton and  $\sigma_T$  is the Thompson cross section. One finds  $L_E \simeq 1.3 \times 10^{46} M_8$  erg s $^{-1}$ , where  $M_8 \equiv (M/10^8 M_\odot)$ . Thus black holes

of masses  $\sim 10^8 M_\odot$ , are needed to power quasars. Further, the Schwarzschild radius  $R_s$  of a black hole is given by  $R_s = 2GM/c^2 \simeq 3 \times 10^{13} M_8$  cm. Thus a characteristic time of variation  $t_v$ , which may be associated with a region of this size is  $\sim R_s/c \simeq 10^3 M_8$  s. This agrees fairly well with the variability time scale observed in the X-ray part of the spectrum for some sources.

Another way of estimating the mass of the black hole is to attribute the observed widths of 5000–10 000 km s<sup>-1</sup> of the emission lines to the Keplerian motion of the gas. One finds that at a distance  $R \simeq 900 R_s$ , the Keplerian velocity is of  $\sim 10^4$  km s<sup>-1</sup>. The absence of broad forbidden lines constrains the electron density in the broad line emission region to  $\sim 10^{10}$  cm<sup>-3</sup> and the temperature to a few times  $10^4$  K. The observed luminosity in any of the emission lines is much less than would be expected from a region of the size  $\sim R$  and further that it cannot exceed the luminosity of a black body at this temperature. This has two fall outs: first, that  $R \gtrsim 10^{15}$  cm and  $M > 10^7 M_\odot$  and second that the region of size  $R$  is not uniformly filled with gas. It exists in the form of filaments exhibiting several zones of varying density and temperature. Particularly, two phases with  $T \simeq 10^8$  K and  $10^4$  K have been shown to be able to coexist in pressure and radiative equilibrium (McCray, 1979; Rees, 1984) (for a review see Osterbrock and Mathews, 1986).

The continuum emission of a quasar can be approximated by a power law. The flux  $F_\nu$  at a frequency  $\nu$  goes as  $\nu^{-\alpha}$  consisting of several components: in the low-frequency ( $\nu \lesssim 1$  GHz) radio region,  $\alpha \simeq 0.1$ ; in the X-ray region  $\alpha \lesssim 0.7$ . The entire spectrum when fitted with an average value of  $\alpha \simeq 1$  shows bends in the radio, bumps in the blue and distinct variations in the hard X-ray and  $\gamma$ -ray regions. The continuum originates very near the black hole and then interacts with the surrounding gas, which as a result, exhibits phases of diverse temperatures and densities.

The radio emission associated with quasars typically has two distinct components: a compact source coincident with the optical emission showing a flat or complex spectrum and, extended roughly symmetrical double radio sources on both sides of the optical object with a spectral index  $\sim 0.7$ . This extended emission can exist out to hundreds of kiloparsecs and is usually seen as two-sided lobes, though only one of the jets feeding the lobes is usually visible. How the central object feeds and maintains these huge jets has remained an issue of active consideration.

The compact central radio sources often appear to be expanding with velocities larger than that of light, the so-called superluminal expansion. This is an apparent effect and results from the relativistic motion of the radio core towards the observer. Jet-like structure is also seen to be associated with optical emission, e.g., in the quasar 3C273, the present extension of the optical jet  $\simeq 30$  kpc from the central object tells us that the quasar phase has existed at least for  $\sim 30$  kpc c<sup>-1</sup>  $\sim 10^6$  years though longer lifetimes are also demanded (Scheuer, 1995). At a typical apparent luminosity  $\sim 10^{47}$  erg s<sup>-1</sup>, total energy released in the quasar phenomenon is  $\sim 10^{60}$ – $10^{61}$  ergs and it has to be produced in a small nuclear region, which again is a pointer to the gravitational nature of the energy release mechanism. The

emission in the optical to the soft X-ray part of the spectrum shows a maximum and is known as the big blue bump. It constitutes contributions from broad and narrow emission lines in addition to the thermal and nonthermal emission from an accretion disk. The X-ray emission again points to the presence of several phenomena taking place cospatially. Attempts have been made to generate a coherent picture of the entire electromagnetic spectrum by joining and superimposing the contributions from different physical processes. The presence or absence of correlated time variability among the different spectral regions gives more clues to the nature of this highly complex phenomena. Studies of polarization of radiation have offered ways to distinguish one process from the other.

The above account, I hope, will serve as a zeroth-order introduction to the phenomenon of quasars for the uninitiated. There are other objects also considered active galactic nuclei such as BL Lacs, Seyfert galaxies and radio galaxies, etc., which have some of their properties similar to those described above along with other essentially different characteristics. For example BL Lacs have weak or no emission lines, are highly polarized and variable. Efforts are on to make unified models in which the various objects have an identifiable underlying common structure and the differences are attributed to a combination of the orientation effects, presence or absence of gas and the relativistic beaming considerations (Antonucci, 1993; Urry and Padovani, 1995).

In this review, the generation of the continuum, its polarization and intensity variability, its interaction with the line emitting gas and the consequent spectral modulation will be discussed with an emphasis on the role of plasma processes. The inclusion of these processes has revealed a new way of interpreting the multifaceted nature of the observations of quasars and their kith and kin.

The observational characteristics of the continuum emission of AGN are described in Section 2. Early models of the continuum radiation are discussed in Section 3. The general theory of plasma parametric processes is summarized in Section 4. The application of parametric decay instability in AGN and quasars is discussed in Section 5. The role of nonlinear stimulated Raman and Compton scattering processes in quasars are discussed in Section 6. Several plasma mechanisms for time variability are described in Section 7. The production of the nonthermal continuum is discussed in Section 8. The review ends with reflections in Section 9.

## 2. Continuum Emission of Active Galactic Nuclei

As mentioned above, active galactic nuclei emit over the entire electromagnetic spectrum beginning from a few hundred MHz to TeV  $\gamma$ -rays. The flux  $F_\nu$  at a frequency  $\nu$  is believed to vary as  $\nu^{-\alpha}$  where  $\alpha$  is the spectral index and has different values in different parts of the spectrum. Attempts to join smoothly the various spectral regions in order to see if there is any continuity, have revealed the existence of bends, bumps, and breaks.

In the radio region, two types of AGN have been identified: these are called radio loud and radio quiet. They look similar in the frequency range  $10^{12}$ – $10^{18}$  Hz but differ significantly at frequencies below  $\sim 10^{12}$  Hz. Radio loud quasars have a compact core of radio emission along with prominent jet emission. The core emission has a flat spectrum with  $\alpha \simeq 0.1$  in the interval  $\nu \sim 10^9$ – $10^{12}$  Hz and  $\alpha \simeq 1$  for  $\nu > 10^{12}$ – $10^{15}$  Hz. The radio luminosities span a huge range and in some sources it may be as high as  $10^{46}$  erg s $^{-1}$  and varies over time scales of days to years. The flat spectrum sources usually possess polarizations of a few percent. The belief is that radio radiation is generated via synchrotron process, that the flat spectrum results from the superposition of several power law spectra, and that the low degree of polarization is due to depolarization effects intrinsic and extrinsic to the source. These sources appear to undergo superluminal expansion, an apparent effect explainable by the near speed of light motion of the radio source towards an observer. More detailed accounts of these sources can be found in Phinney (1985), Stein and O'Dell (1985), and Marscher (1992).

Radio quiet AGNs have very little emission at  $\nu < 10^{12}$  Hz and what little there is, probably comes from an extended region. They might possibly be mildly relativistic jets which suffer rapid expansion and radiative losses and cannot be seen at large distances from the nucleus (Mannheim, 1994). Unified schemes for radio quiet AGN depend mainly upon the obscuration produced by a dusty torus, which prevents the broad line region and most X-ray emission from being seen if the angle of the line of sight to the symmetry axis is too large, thereby explaining the dominant differences between type 1 and type 2 Seyfert galaxies (e.g., Antonucci, 1993). The fundamental differences between radio quiet and radio loud AGN remain uncertain; the amount of spin of the black hole might play an important role (Wilson and Colbert, 1995).

The picture for high-frequency emission from radio-loud objects has not undergone any significant change since it was first proposed by Jones et al. (1974). Non-thermal synchrotron processes account for radiation from radio to ultraviolet region and the hard X-rays and gamma-rays originate through the upscattering of low-frequency photons via inverse Compton processes (Bregman, 1990, 1994).

In radio-quiet AGN, the far-infrared (FIR) spectrum shows a steep rise from millimeter to the far-infrared with a spectral index  $\alpha \gtrsim 2.5$ , which attains a value  $\sim (1)$  beyond the FIR. Out of the three possible ways of producing mm-FIR radiation, i.e., synchrotron, non-thermal power law, and thermal emission from dust, the last seems to account for most of the properties in this region.

Beyond the IR, the emission in the optical-ultraviolet – soft X-ray region is often referred to as the big blue bump. This spectral region provides the absolute maximum in the power output of many of these sources and contains typically one-third to one-half of the total observed power. In addition to the continuum from say  $1\mu$  to 0.5 keV, the big blue bump has also contributions from Fe II emission lines as well as hydrogen recombination radiation. Until recently, the most favoured explanation for this part of the spectrum was the thermal emission

from an accretion disk, joining on to a nonthermal power law for the near-infrared emission (Malkan, 1991). However, the realization that thermal emission from dust may be the dominant process for infrared emission, has made the pure accretion disk model suspect. Further, the black-hole accretion disk models predict a time lag of  $\sim$  weeks between the UV and optical variations, whereas the observations put an upper limit of a few days. Signatures of rotation associated with an accretion disk have also not been confirmed yet (Bregman, 1994). Barvainis (1993) has proposed optically thin free-free emission for the optical UV continuum. Since it is a broad-band emission mechanism, the time delay issue is taken care of. The X-ray emission region covers the 0.1–100 keV range. The high-frequency extension (0.1–1 keV) of the big blue bump is referred to as the soft excess. The region 1–100 keV exhibits a power-law continuum with energy index  $\sim$  0.9. Models based on photon-photon collisions mediating electron positron pair production as well as those depending on inverse Compton scattering have been proposed. Studies near the electron-positron annihilation line (0.511 MeV) can differentiate between these models.

Gamma-ray emission in the GeV–TeV range has been observed only in radio-loud AGN and appears to be well correlated with radio emission. Variability time scales of the order of a few days are seen. The question of predominance or otherwise of gamma-ray power in the power distribution of these sources is being raised and many more observations are needed before it could be answered with any degree of confidence.

### 3. Early Models of Continuum Emission

The core radio radiation from AGN is believed to be produced via synchrotron process in which relativistic electrons gyrate in an ambient magnetic field. The synchrotron radiation mechanism has been discussed in various astrophysical contexts and the characteristics of the radiation so produced are well documented (Pacholczyk, 1970; Ginzburg and Syrovatskii, 1974; Rybicki and Lightman, 1979). For a power-law energy distribution of electrons, synchrotron radiation flux also has a power-law spectral distribution with  $\alpha = (\beta - 1)/2$ , where  $\beta$  is the energy index ( $f(E) \propto E^{-\beta}$ ) of the electrons. It is found that many of the acceleration processes like shock acceleration, acceleration by magnetohydrodynamic waves, etc., produce a value of  $\beta \sim 3$ . This, then gives a value of  $\alpha \simeq 1$  which is close to the observed radio spectrum up to a low-frequency turnover. At this turning point, the electrons begin to absorb the radiation they emit and the source is said to be self-absorbed. The radio flux varies as  $f_\nu \propto \nu^{5/2}$  for frequencies below the turning point. Now this spectral shape has rarely been observed; instead, a flat spectrum with  $\alpha \simeq 0.1$ –0.3 is what is often observed. This is explained by invoking the inhomogeneous nature of the radio source, wherein a tailored superposition of  $\nu^{5/2}$  spectra gives rise to a flat spectrum.

The self-absorption occurs when  $T_B \sim (\gamma/K_B)m_e c^2 \sim 10^{10}\gamma$  where  $\gamma$  is the Lorentz factor of the synchrotron emitting electrons,  $K_B$  is the Boltzmann constant and  $m_e$  is the electron mass.  $T_B$ , the brightness temperature at a frequency  $\nu$  is defined as  $K_B T_B = c^2 F_\nu / 2\pi\theta^2\nu^3$ , where  $F_\nu$  is the radiative flux and  $\theta$  is the angular size of the source. From the observed values of  $F_\nu$ ,  $\nu$  and  $\theta$  at the turnover frequency, one can determine the Lorentz factor  $\gamma$  of the electrons emitting at the turnover frequency. Since the synchrotron turnover occurs at a frequency  $\nu \simeq \gamma^2(0.3eB/2\pi mc(1+z))$  one can determine the magnetic field  $\mathbf{B}$  for a known value of the redshift  $z$ , and then the total number of relativistic electrons required to account for the observed value of  $F_\nu$ . Thus from the self-absorbed feature of the spectrum, typical values of the physical parameters of the radio emitting plasma can be estimated. The variability aspect of the radio emission will be discussed in a later section.

Linear polarization as high as 75% is predicted by the synchrotron mechanism and high linear polarization is often seen in extended radio sources. The compact radio sources, however show polarization of a few percent. Thus, depolarization processes are usually supposed to be operative. With faith in the synchrotron mechanism, thus restored, it was proposed that, at least in radio-loud objects, radio to ultraviolet (and sometimes soft X-ray) radiation is produced by synchrotron process and X-rays to gamma rays are produced through the inverse Compton scattering of the synchrotron produced IR-UV photons by the synchrotron emitting electrons (Hoyle et al., 1966). The power  $P_{sy}$  emitted per electron by the synchrotron mechanism is given by (Rybicki and Lightman, 1979)

$$P_{sy} = \frac{2}{3c}\sigma_T\gamma^2\beta^2B^2, \quad (3.1)$$

where  $\sigma_T$  is the Thomson cross-section,  $\beta c$  is the perpendicular velocity of the relativistic electron with Lorentz factor  $\gamma$  perpendicular to the direction of  $\mathbf{B}$ , the magnetic field. The power  $P_c$  emitted per electron by the inverse Compton process is given by (Rybicki and Lightman, 1979):

$$P_c = \frac{2}{3c}\sigma_T\gamma^2\beta^24\pi U_{rad}, \quad (3.2)$$

where  $U_{rad}$  is the energy density of the synchrotron generated photons.

It was argued by Hoyle et al. (1966) that the ratio  $P_c/P_{sy}$  turns out to be much larger than one, in fact  $\sim 10^5$  at a frequency  $\nu = 10^{14}$  Hz for 3C273, and similarly for other objects. This implied that the Compton process generated much more power by using synchrotron photons and electrons than did the synchrotron process, leading to a divergence in which the inverse Compton process acts on itself to produce higher power at higher and higher frequencies. This dilemma is known as Compton catastrophe. Jones et al. (1974), however, have criticized this conclusion, for according to them spectral power instead of the total power should be compared since the former is what the observations provide. Further, the relative

contribution of the synchrotron self-Compton (SSC) process can be reduced for anisotropic distribution of relativistic electrons in ordered magnetic fields. Another way out of the Compton catastrophe is to assume different values of the Lorentz factor for producing radiation at different frequencies. After all, it is the energy in the relativistic electrons that is converted into high-frequency radiation. However, for a population of electrons with a single value of the Lorentz factor, one can demand that  $U_{\text{rad}} \lesssim B^2/4\pi$  in order to avoid Compton catastrophe.

If  $L$  is the luminosity and  $d$  the size of the source,  $L = \pi d^2 c U_{\text{rad}} = 4\pi R^2 F$ , where  $F$  is the flux received at the Earth from the object at a distance  $R$ . Thus  $U_{\text{rad}} = 4F/\theta^2 c = 8\pi(\nu^3/c^3)K_B T_B < B^2/4\pi$  gives an upper limit for the brightness temperature  $T_B \sim 10^{12}-10^{13}$  K. Detection of rapid variability (small  $\theta$ ) in some sources implies, then, that the brightness temperatures, in these sources, can exceed the SSC limit by several orders of magnitude. This difficulty has been resolved by suggesting that the source is expanding relativistically toward the observer (Rees, 1966). The time scale for variability in the source's rest frame then increases by the Kinematic Doppler factor  $\delta \equiv [\gamma_0(1 - \beta_{||0})(1 + z)]^{-1}$  and so does the angular size of the source, which results in the reduction of the brightness temperature. Thus relativistic beaming has been found handy for explaining the observed superluminal expansion, the low-frequency variability, and rapid changes in polarization and intensity in addition to providing; a cure for the Compton catastrophe.

Thus the scenario that is popular for the radio-loud and other related objects consists of a jet-like structure, emanating from the core. The radiation from radio to UV and sometimes even including X-rays is produced through incoherent non-thermal synchrotron process. Time variability studies provide an estimate of the relative sizes of the emission regions at various frequencies. In some other sources X-rays may be generated by the inverse Compton scattering of low-frequency photons. If this process operates then one expects to see correlated variability in the seed photons at infrared and millimeter wavelengths and the Compton scattered photons at X-rays. The overall spectrum has a spectral index close to unity with a very broad peak in the millimeter to ultraviolet region. This feature has a large range in wavelength and probably reflects the range in the parameters of the radiating plasma. Typical values of the parameters may lie in the range  $B \sim 10^2-10^4$  G, relativistic electron density  $n \sim 10^8-10^{10}$  cm $^{-3}$ , Lorentz factor  $\gamma \sim 10^3-10^4$  and the size of the emission region  $d \sim 10^{15}-10^{17}$  cm. This plasma can provide a luminosity  $L \sim 10^{44}-10^{46}$  erg s $^{-1}$ . The Compton limited luminosity is also of the same order. Recent observations from Compton Gamma-Ray observatory have revealed a surprising correlation between emission at GeV and radio frequencies. This lends credence to the inverse Compton scattering process for the generation of gamma-rays (Marscher and Bloom, 1992). The observed GeV energies of  $\sim 10^{48}$  erg s $^{-1}$  are perhaps the results of relativistic beaming. Time variability of the order of a few days has been seen in gamma-rays, also typical of the optical and UV region, again pointing to the role of upscattering processes (Kniffen et al., 1993).

None of the radio-quiet objects have been seen to emit GeV photons. As mentioned already, the radio quiet objects have very weak emission of the order of a few milliJansky at frequencies  $\simeq 10^{10}$  Hz and the emission rises thousand fold to the level of Jansky at far-infrared wavelengths. This steep fall with an average slope of 3.75 (Hughes et al., 1993) towards low frequency cannot be accounted by synchrotron–self-absorption mechanism which can, at best produce a fall with a slope of 2.5. In addition a new component in the form of a bump between 2–10  $\mu\text{m}$  lying above the underlying power law has been identified (Robson et al., 1986; Edelson and Malkan, 1986). It has been suggested that hot dust may be responsible for most of the infrared emission in radio-quiet objects (Rees et al., 1969; Rieke, 1978; Barvainis, 1987).

Dust is thus assumed to be present in sources displaying the infrared bump. It absorbs the optical-ultraviolet radiation from the central continuum and re-emits at infrared wavelengths. The power  $P_\nu$  per unit frequency emitted by a single grain at a temperature  $T_g$  is given by (Barvainis, 1987):

$$P_\nu = 4\pi a^2 \pi Q_\nu B_\nu(T_g) \text{ erg s}^{-1} \text{ Hz}^{-1}, \quad (3.3)$$

where  $a$  is the size of a grain and is believed to be of the order of 0.05  $\mu\text{m}$ ,  $Q_\nu$  is the absorption efficiency of the grains in the infrared and  $B_\nu(T_g)$  is the Planck function. A grain exposed to UV radiation will achieve equilibrium when the rate of absorption in the UV equals its rate of emission in the infrared, i.e.,

$$\pi a^2 \int U_\nu c Q_{uv} d\nu = \int P_\nu d\nu, \quad (3.4)$$

where ( $Q_{uv}\pi a^2$ ) is the absorption cross-section of a grain and  $U_\nu$  is the energy density in the ultraviolet. This equality determines the temperature of a grain. One can also determine the distance  $\xi$  from the central source at which the temperature  $T_g \gtrsim 1500$  K, which is the evaporation temperature of graphite grains. The optically thin radiation from graphite grains at  $T_g \simeq 1500$  K peaks at  $\sim 2$   $\mu\text{m}$  and is suggestive of the infrared bump. The size of the dust region can be determined by acknowledging that at large distances from the UV source, the dust does not absorb enough UV and remains cold and nonradiating in the infrared. Thus the infrared emission is supposed to originate in a region of  $\simeq 10$  pc extent situated about a pc from the central UV source. Predominantly graphite grains of  $\sim 0.05$   $\mu\text{m}$  size, either distributed spherically symmetrically or in clumps with a total mass  $\sim 10^3$ – $10^5 M_\odot$ , at a range of temperatures can account for the infrared characteristics of a majority of the radio-quiet objects. It is interesting to recall that the flat radio spectrum was produced by assuming that the synchrotron self-absorbed source is made up of several different components and here, the steep infrared spectrum is produced by assuming that the emission region consists of dust at many different temperatures! Are there other interpretations?

Advancing towards high frequencies next, comes the big blue bump spread over from 1  $\mu\text{m}$ –0.5 keV region. It is believed that this spectral region consists of two

components, a nonthermal power-law radiation with a spectral index  $\alpha \simeq 1$  over which lies superimposed thermal emission with a black-body spectrum modified due to the spatial variation of the temperature of the emitting region. The flux  $F_a$  released per unit area from the matter accreted at a rate  $\dot{M}$  on to a black hole of mass  $M_H$  is given by (Shields, 1978)

$$F_a \approx \frac{3GM_H\dot{M}}{8\pi r^3}. \quad (3.5)$$

If most of this power is radiated as if from a black body then the corresponding black-body temperature  $T_a$  is found to be

$$T_a(r) = \left( \frac{F_a}{4\pi\sigma} \right)^{1/4}, \quad (3.6)$$

where  $\sigma = 5.67 \times 10^{-5} \text{ erg s}^{-1} \text{ cm}^{-2} \text{ K}^{-4}$ .

The frequency of maximum emission at a radius  $r$  can be determined from

$$\nu_{\max}(r) = \frac{2.8K_B T_a(r)}{h}. \quad (3.7)$$

Integrating  $F_a$  over the area, taking  $r_{\min}$  as the inner radius of the accretion disk, one finds the energy emitted per sec per Hz,  $f$ , to be (Shields, 1978)

$$\begin{aligned} f &\sim \frac{1}{\nu_{\max}(r_{\min})} \int_{r_{\min}}^{\infty} F_a r \, dr = \\ &= \left[ \frac{3GM_H\dot{M}\sigma^{1/2}}{8\pi} \right]^{2/3} \left( \frac{2.8K_B}{h} \right)^{-4/3} \nu_{\max}^{1/3}(r_{\min}). \end{aligned} \quad (3.8)$$

Thus the flux  $f$  has a spectral index  $\alpha = -\frac{1}{3}$ . Of course at each spatial point the gas emits a Planckian and the  $(\frac{1}{3})$  spectrum results from the spatial variation of the temperature and therefore of the frequency of the maximum emission. For frequencies larger than  $\nu_{\max}$ , the thermal emission falls off exponentially. This, in essence, is the thermal accretion model of the big blue bump, which lies over the nonthermal continuum extending from far infrared to X-rays. Several variants of this model have been proposed including contributions from dust, but it appears that if the near-infrared emission is not nonthermal and is due to dust emission, it may be difficult to save the accretion model (Malkan, 1991, 1992; Czerny, 1994).

An alternative proposal is that the optical UV bump can be accounted by the free-free emission from an optically thin region. The free-free emissivity is given by (Barvainis, 1993)

$$\epsilon_\nu = 5.4 \times 10^{-39} Z^2 \frac{n_e n_i}{T^{1/2}} g(\nu, T) e^{-h\nu/KT} \text{ ergs s}^{-1} \text{ cm}^{-3} \text{ Hz}^{-1} \text{ rad}^{-2}, \quad (3.9)$$

where  $Z$  is the nuclear charge,  $g(\nu, T)$  is the Gaunt factor, and  $n_e$  and  $n_i$  are electron and ion densities, respectively. The luminosity  $L$  can be calculated as

$$L = 4\pi\nu\epsilon_\nu V, \quad (3.10)$$

where  $V$  is the volume of the source. If  $R$  is the size of the source, then the free-free absorption optical depth  $\tau_\nu$  is found to be

$$\tau_\nu = R\alpha_\nu = \frac{R\epsilon_\nu}{B_\nu(T)}, \quad (3.11)$$

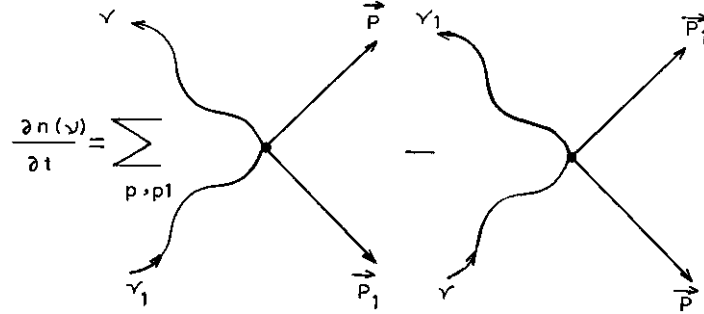
where  $\alpha_\nu$  is the free-free absorption coefficient and  $B_\nu(T)$  is the Planck function. In the optical-UV region ( $\nu \sim 10^{15}$  Hz), a source consisting of a large number ( $\sim 10^{13}$ ) of high electron density ( $\sim 10^{15} \text{ cm}^{-3}$ ) clouds at temperature  $\sim 10^5$ – $10^6$  K spread over a region  $L \sim 10^{16}$  cm can account for the required luminosity  $L \sim 10^{46} \text{ erg s}^{-1}$ . The free-free flux spectrum is much broader than that of a black body and is suggested to be in closer agreement with observations. This model also accommodates the small size attributed to the big blue bump from microlensing considerations.

The X-ray emitting region in the energy range 0.1–100 keV probably lies interior to the big blue bump. The rapidly falling low energy branch (0.1–1 keV) perhaps seen as the soft X-ray excess, could be identified with the high-frequency extrapolation of the big blue bump. The emission in 1–100 keV range is in the form of a power law with  $\alpha \simeq 0.7$ . The proposed mechanisms of X-ray emission are the thermal and nonthermal Comptonization of low-frequency photons and the electron positron pair production and annihilation processes.

In thermal Comptonization, X-rays are generated when soft photons are upscattered by a thermal distribution of hot electrons. Through this process, photons with average energy  $\epsilon_f \sim e^Y \epsilon_i$  are produced when soft photons of energy  $\epsilon_i$  suffer multiple scatterings by thermal electrons. The Compton parameter  $Y$  is the product of average fractional energy gain per scattering and the total number of scatterings, which is equal to the electron scattering optical depth for an optically thin medium and equal to the square of the optical depth for an optically thick medium. In an electron distribution of temperature  $T$  and optical depth  $\tau$ , the Compton parameter  $Y$  is given as

$$Y = \frac{4K_B T}{m_e c^2} \text{Max}(\tau, \tau^2). \quad (3.12)$$

The time evolution of the photon phase space density  $n(\nu)$  can be studied by using the Boltzmann equation for Compton scattering shown below:



$$= c \int d^3 p \frac{d\sigma}{d\Omega} d\Omega [f_e(p_1)n(\nu_1)(1+n(\nu)) - f_e(p)n(\nu)(1+n(\nu_1))] \quad (3.13)$$

(Rybicki and Lightman, 1979; Harris, 1975). Here the differential scattering cross section for Compton scattering is given by

$$\frac{d\sigma}{d\Omega} = \frac{3\sigma_T}{4\pi}(1 + \cos^2 \theta) \quad (3.14)$$

with  $\sigma_T = (e^2/mc^2)^2$  and  $\theta$  is the scattering angle of the photon. The probability for the absorption of a photon of frequency  $\nu$  is  $n(\nu)$  and the probability for emission of a photon of frequency  $\nu$  is  $[1 + n(\nu)]$ ;  $f_e$  is the electron distribution function and  $n(\nu)$  is related to the spectral energy density  $\epsilon_\nu$  of radiation in  $\text{erg cm}^{-3} \text{Hz}^{-1}$  as

$$n(\nu) = \frac{c^3 \epsilon_\nu}{8\pi h\nu^3}. \quad (3.15)$$

To second order in the change in photon energy ( $\nu_1 - \nu$ ) for a Maxwellian distribution of electrons with temperature  $T$ , one finds the time evolution of the photon density  $n(\nu)$  as

$$\frac{\partial n(\nu)}{\partial t_c} = \left(\frac{K_B T}{m_e c^2}\right) \frac{1}{x^2} \frac{\partial}{\partial x} (x^4 (n' + n + n^2)), \quad (3.16)$$

where  $x = h\nu/K_B T$ ,  $t_c = (n_e \sigma_T c)t$ ,  $n' = \partial n/\partial x$ .

$n_e$  is the electron density and  $(n_e \sigma_T c)^{-1}$  is the mean time between scatterings. Equation (3.16) is the Kompaneets equation and describes the time evolution of the photon distribution function undergoing multiple inverse Compton scatterings. One can obtain some insight by studying the limiting cases of the Kompaneets equation. For steady state, i.e., for  $\partial n/\partial t_c = 0$ , we find a Wien's type ( $n(x) \propto e^{-x}$ ) saturated spectrum. It can be shown that the total energy  $\epsilon$  increases exponentially with time, i.e.,

$$\epsilon = \int \epsilon_\nu d\nu \simeq \epsilon(0) \exp \left[ \frac{4K_B T}{m_e c^2} \frac{t}{t_c} \right]. \quad (3.17)$$

This is reminiscent of an exponential increase of the single photon energy discussed earlier. The nature of the Compton spectra can be studied for an input photon spectrum  $n(\nu)$  by solving the Kompaneets equation. We give here a few limiting solutions for some special cases. In a thermal distribution of plasma, bremsstrahlung or free-free absorption and emission are also taking place in addition to scattering. One can determine which process is most dominant at a given frequency by comparing the opacities ( $\kappa$ ) for different processes. For example the frequency  $\nu_0$  at which electron scattering ( $\kappa_{es}$ ) and free-free absorption ( $\kappa_{ff}$ ) are equal can be found from  $\kappa_{es} = \kappa_{ff}$ . All photons of frequencies lower than  $\nu_0$  will not be subjected to strong scattering. Then, there is the frequency  $\nu_t$  at which the medium becomes optically thin ( $\tau_{cs}$ ) which can be determined from  $\kappa_{es} = \kappa_{ff} \tau_{es}^2$ . Photons of frequency larger than  $\nu_t$  will not suffer strong absorption. In the range  $\nu_0 < \nu < \nu_t$  both scattering and absorption are important. Further, inverse Compton scattering is important at frequencies  $> \nu_c$  at which the parameter  $Y = 1$ . Thus, in a scattering and absorbing medium, the black body photon spectrum gets modified and becomes closer to the Wien spectrum for  $Y \gg 1$ . The complete spectrum of radiation from a thermal medium participating in the free-free emission and absorption and saturated inverse Compton scattering has been shown in Figure 7.4 of Rybicki and Lightman (1979). As discussed earlier, the power  $P_c$  radiated by a single electron (of Lorentz factor  $\gamma$ ) Compton scattering is given by

$$P_c = \frac{4}{3} \sigma_T c \gamma^2 \beta^2 U_{ph} . \quad (3.18)$$

The total power  $P_T$  radiated by a medium of relativistic electrons having a power-law energy distribution  $N(\gamma)$  can then be obtained as

$$P_T = \int P_c N(\gamma) d\gamma , \quad (3.19)$$

where

$$N(\gamma) \propto \gamma^{-p} ,$$

for some range  $\gamma_{\min} < \gamma < \gamma_{\max}$  and zero otherwise. Thus, like the synchrotron process, the Compton spectrum is also of the power-law form and the energy of the scattered photon is  $\sim \gamma^2$  times that of the incident photon. A power-law photon distribution can also result from multiple scatterings off a non-power-law electron distribution.

So, we have all these mechanisms to convert the kinetic energy of electrons and protons into radiation. But what produces these relativistic particles? Electrons and protons in their accretion flow do acquire energies of the order of MeV as they approach a black hole. This fluid flow energy needs to be tapped as, e.g., by viscous dissipation of the Keplerian flows and or the formation of shocks. The thermal models of the continuum X-ray emission imply temperatures  $> 10^9$  K, that is conditions

where  $K_B T \simeq m_e c^2$  must exist. Also relativistic particles in the tails of the distribution function may produce gamma rays of energies larger than MeV. Under these circumstances, electron-positron pair production begins to take place. The medium now consists of electrons, positrons, and protons at ultrarelativistic energies. They produce radiation through thermal, synchrotron, and Compton processes. The produced radiation then gets modified due to propagation in an optically thick or thin medium, as discussed before. But now, there are additional processes of production of electron and positron pairs. The situation becomes more complex and nonlinear. Photons produce pairs and pairs produce photons. One has to determine the steady state emergent luminosity and its spectrum, which will also provide the equilibrium pair density and energy. Further, such a soup of radiation and the three-component plasma may be irradiated from external radiation such as that generated before the pair production began. Detailed discussions of relativistic plasmas can be found in Pacholczyk (1970), Lightman (1982), Svensson (1982, 1984), Rees (1984), Osterbrock and Mathews (1986), Zdziarski et al. (1990), Antonucci (1993), Scheuer (1995), Mushotzky et al. (1993), Urry and Padovani (1995), and Wilson and Colbert (1995). Thus, there are two ways of producing power-law X-ray continuum: inverse Compton scattering of soft photons by thermal or nonthermal electrons and or by the electron-positron-photon processes. The two models can be distinguished by studying the electron-positron annihilation region (0.511 MeV) since they differ in their estimates of annihilation line strength and X-ray continuum shape.

#### 4. Plasma Processes

Although the processes by which the gravitational energy of the accreted matter is converted into relativistic particles, high-temperature plasmas probably consisting of electrons, protons and positrons and electromagnetic radiation are still a matter of speculation and debate, the existence of strongly interacting matter and radiation in the environs of active galactic nuclei has never been doubted. A plasma, by nature is hyperactive. More often than not, it responds violently to external stimuli in an attempt to attain equilibrium. In fact in AGN atmospheres, the possibility of the three-component plasma adds further to the complexity and the multiplicity of the phenomena.

When subjected to strong radiation fields, a plasma exhibits a variety of nonlinear processes which modify its parameters as well as those of the radiation. When the size of the plasma region disturbed by an electromagnetic wave is larger than the mean free path of an electron, an electron can gain a significant amount of energy before suffering collisions with other ions and neutrals. Further, the large mass difference between electrons and other particles hinders the transfer of energy from the electrons to the heavy particles. Thus, the electric field of the electromagnetic wave heats the electrons preferentially, as a result of which the dielectric constant  $\epsilon$  and the electrical conductivity  $\sigma$  of the plasma become functions of the

electromagnetic field and a nonlinear relation between the electric field  $\mathbf{E}$  and the current density  $\mathbf{J} = \sigma(\mathbf{E})\mathbf{E}$  is established. In the opposite case when the size of the disturbed plasma region is much smaller than the mean free path of an electron due to the pressure exerted by the inhomogeneous electric field of the radiation, compressions, and rarefactions form in the plasma medium. This time, the dielectric constant of the plasma becomes a function of the electric field through the density modulation. Summarizing, a collisional plasma becomes nonlinear mainly through the dependence of electron temperature on the electric field and a collisionless plasma becomes nonlinear mainly through the dependence of electron density on the electric field.

Strong radiation incident on a plasma can give rise to other waves through the excitation of charge and current density fluctuations. It is well known that in the linear regime, i.e., for the radiation energy density below a critical value, an electromagnetic wave incident on a plasma suffers reflection if its frequency is near the electron plasma frequency. Whereas, in the nonlinear regime, an electromagnetic wave can decay into an electron plasma wave and an ion-acoustic wave and undergo absorption instead of reflection. Thus a reflecting medium becomes an absorbing medium under the action of strong radiation. On the other hand, if the frequency of the incident radiation is larger than the electron plasma frequency, the medium is transparent, in the linear regime, whereas, in the nonlinear case, the incident wave can decay into an electron plasma wave and another electromagnetic wave, propagating preferentially in a direction opposite to that of the incident wave. So, here again, a transparent medium becomes reflecting under the action of strong radiation.

Thus strong radiation propagates in a plasma in different and novel ways by a stimulated generation of waves that a plasma can support. Since the entire system of plasma particles participates in a correlated fashion, the wave excitation processes and the accompanying scattering and absorption processes are much more efficient than the single particle processes. The electromagnetic wave is said to undergo anomalous absorption, scattering and stimulated emission under favourable circumstances. The role of these processes in the generation of the AGN continuum and its interaction with the surrounding plasmas like that in accretion disks and the broad line regions has received some attention in the last decade or so. Before taking up the specific applications to AGN, the mathematical tools needed to investigate the interaction of strong radiation with a plasma will be summarized.

#### 4.1. PLASMA-RADIATION COUPLING

It is well known that an unmagnetized plasma supports three types of normal modes (Chen, 1974):

- (1) an electromagnetic wave ( $\omega_s, K_s$ ) described by the linear dispersion relation:

$$\omega_s^2 = \omega_{pe}^2 + K_s^2 c^2 ; \quad (4.1)$$

(2) an electrostatic electron plasma ( $\omega_e, \mathbf{K}_e$ ) wave described by the linear dispersion relation:

$$\omega_e^2 = \omega_{pe}^2 + \frac{3}{2} K_e^2 V_e^2, \quad (4.2)$$

and (3) an electrostatic ion-acoustic wave ( $\omega_i, \mathbf{K}_i$ ) with linear dispersion relation:

$$\omega_i^2 = \frac{\omega_{pi}^2 K_i^2 \lambda_{De}^2}{1 + K_i^2 \lambda_{De}^2}, \quad (4.3)$$

$$\simeq \omega_{pi}^2 \quad \text{for } K_i \lambda_{De} \gg 1,$$

$$\sim K_i^2 C_s^2 \quad \text{for } K_i \lambda_{De} \ll 1.$$

Here,  $\omega_{PJ} = (4\pi n_j e^2 / m_j)^{1/2}$  is the plasma frequency,  $V_j = (2K_B T_j / m_j)^{1/2}$  is the thermal velocity,  $\lambda_{Dj} = (K_B T_j / 4\pi n_j e^2)^{1/2}$  is the Debye length,  $C_s = (K_B T_e / m_i)^{1/2}$  is the sound speed,  $n_j$ ,  $m_j$ , and  $T_j$  are the density, the mass and the temperature of the particles of the  $j$ th species where  $j = e$  for electrons and  $i$  for ions.

When an electromagnetic wave of large amplitude propagates through a plasma, it can couple with one or more of the three normal modes. The type of interaction is governed by the energy and momentum conservation laws. In addition, the amplitude of the incident electromagnetic radiation must exceed a threshold value. Thus, depending upon the frequency ( $\omega_0, \mathbf{K}_0$ ) of the radiation incident on a plasma, one or more of the following interactions can occur:

(1) The incident electromagnetic wave ( $\omega_0, \mathbf{K}_0$ ) can decay into an electron plasma wave ( $\omega_e, \mathbf{K}_e$ ) and an ion-acoustic wave ( $\omega_i, \mathbf{K}_i$ ) such that

$$\omega_0 = \omega_e + \omega_i \quad \text{and} \quad \mathbf{K}_0 = \mathbf{K}_e + \mathbf{K}_i.$$

This process is known as the Parametric Decay Instability (PDI) (Figure 1). Here the entire electromagnetic energy is converted into the electrostatic energies of the electron plasma wave and the ion-acoustic wave, to the first order. Therefore parametric decay instability is an absorption process and could turn out to be much more efficient than the collisional absorption due to electron ion Coulomb collisions.

(2) The incident electromagnetic wave ( $\omega_0, \mathbf{K}_0$ ) can decay into another electromagnetic wave ( $\omega_s, \mathbf{K}_s$ ) and an electron plasma wave ( $\omega_e, \mathbf{K}_e$ ) such that

$$\omega_0 = \omega_s + \omega_e \quad \text{and} \quad \mathbf{K}_0 = \mathbf{K}_s + \mathbf{K}_e.$$

This process is known as stimulated Raman scattering (SRS) (Figure 2). Here, a part of the incident electromagnetic energy appears as a scattered electromagnetic wave ( $\omega_s, \mathbf{K}_s$ ) and the rest goes into the electrostatic energy of the electron-plasma

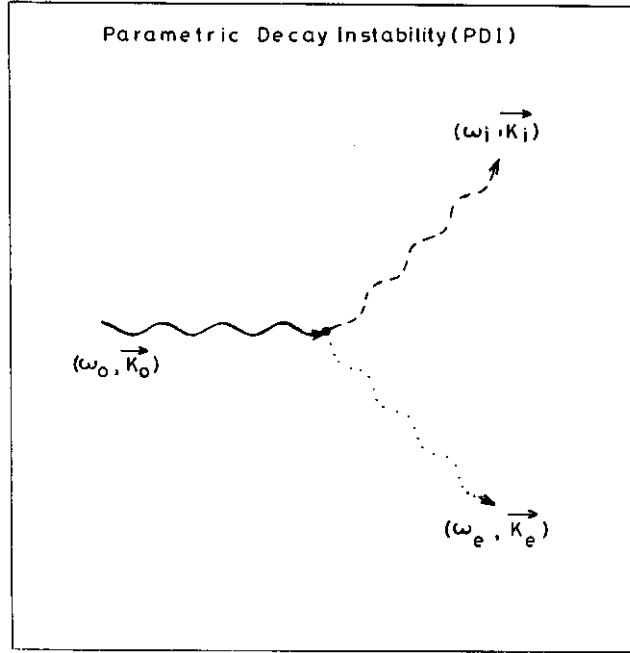


Figure 1. An incident electromagnetic wave  $(\omega_0, \mathbf{K}_0)$  decays into an electron-plasma wave  $(\omega_e, \mathbf{K}_e)$  and an ion-acoustic wave  $(\omega_i, \mathbf{K}_i)$ .

wave, which will be eventually absorbed in the plasma. Thus this is a scattering as well as an absorbing process.

(3) The incident electromagnetic wave  $(\omega_0, \mathbf{K}_0)$  can decay into another electromagnetic wave  $(\omega_s, \mathbf{K}_s)$  and an ion-acoustic wave  $(\omega_i, \mathbf{K}_i)$  such that

$$\omega_0 = \omega_s + \omega_i \quad \text{and} \quad \mathbf{K}_0 = \mathbf{K}_s + \mathbf{K}_i .$$

This process is known as stimulated Brillouin scattering (SBS) (Figure 3). This is also a scattering accompanied by an absorption process. Of course SRS and SBS operate in different regimes of plasma and radiation parameters with a possibility of an overlap.

(4) The incident electromagnetic wave  $(\omega_0, \mathbf{K}_0)$  can decay into two electron-plasma waves,  $(\omega_{e1}, \mathbf{K}_{e1})$  and  $(\omega_{e2}, \mathbf{K}_{e2})$  such that

$$\omega_0 = \omega_{e1} + \omega_{e2} \quad \text{and} \quad \mathbf{K}_0 = \mathbf{K}_{e1} + \mathbf{K}_{e2} .$$

This process is known as the Double Plasma Decay Instability (DPDI) (Figure 4) and is an absorption process. It will occur if  $\omega_0^2 \simeq 4\omega_e^2$ , i.e., if the plasma density  $n$  is a quarter of the critical density  $n_c$  defined as  $\omega_0^2 = 4\pi n_c e^2 / m_e$ . Such a region of a plasma is known as the quarter critical region. Since the frequency of the incident radiation  $\omega_0$  must be equal to or greater than the electron plasma frequency for the

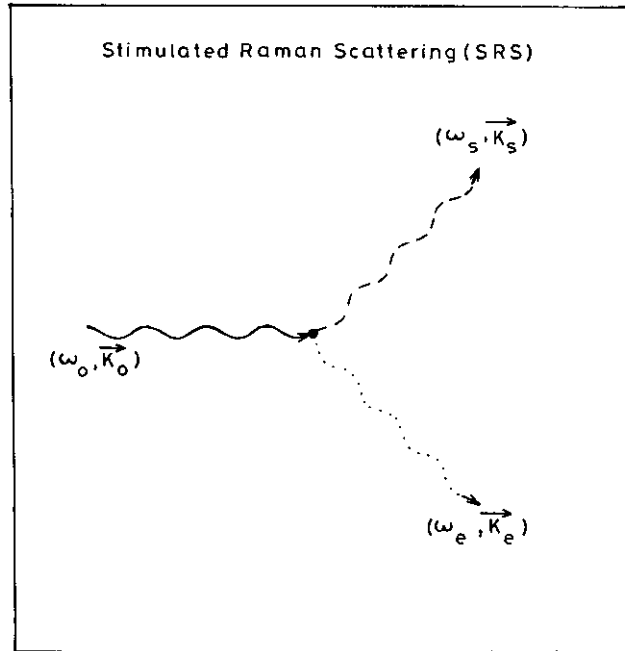


Figure 2. An incident electromagnetic wave  $(\omega_0, \vec{k}_0)$  decays into an electron-plasma wave  $(\omega_e, \vec{k}_e)$  and a scattered electromagnetic wave  $(\omega_s, \vec{k}_s)$ .

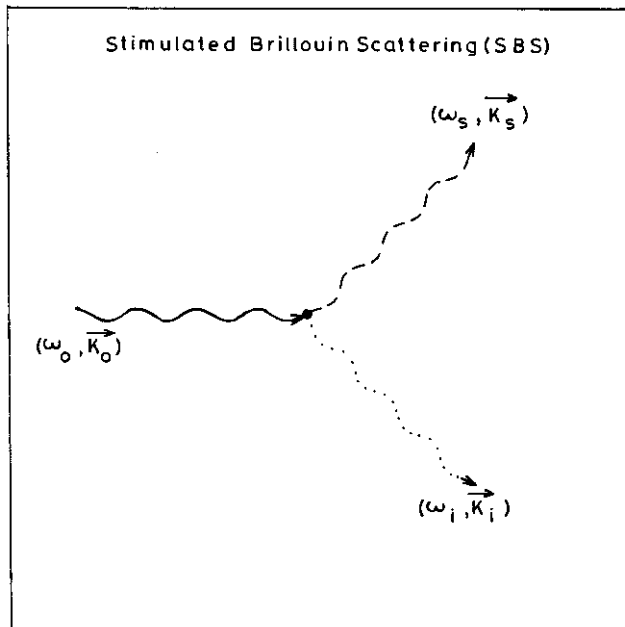


Figure 3. An incident electromagnetic wave  $(\omega_0, \vec{k}_0)$  decays into an ion-acoustic wave and a scattered electromagnetic wave  $(\omega_s, \vec{k}_s)$ .

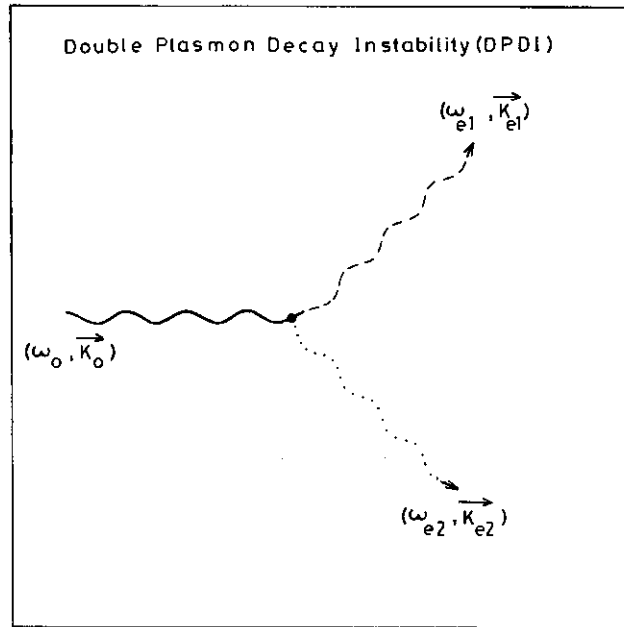


Figure 4. An incident electromagnetic wave  $(\omega_0, \mathbf{K}_0)$  decays into two electron plasma waves  $(\omega_{e1}, \mathbf{K}_{e1})$  and  $(\omega_{e2}, \mathbf{K}_{e2})$ .

wave to propagate into a plasma, the double ion decay process, i.e.,  $\omega_0 = \omega_{i1} + \omega_{i2}$  cannot occur.

All these processes are instabilities since both the decay products, electrostatic as well as electromagnetic waves, grow in amplitude in an exponential manner and the growth rate depends on the amplitude of the incident radiation, among other factors.

#### 4.2. THE INSTABILITY MECHANISM

When a large amplitude  $(\omega_0, \mathbf{K}_0, \mathbf{E}_0)$  plane polarized electromagnetic wave (the pump) propagates through a non-relativistic plasma, the electrons and ions begin to oscillate with velocity  $\mathbf{u}_{0j} = e_j \mathbf{E}_0 / m_j \omega_0$  in the incident electric field  $\mathbf{E}_0$ .

Now, plasmas always have propagating density perturbations  $\delta n_j(\mathbf{K}, \omega)$  which due to their velocities  $\mathbf{u}_j$  produce currents  $\delta \mathbf{J}_j(\omega_0 \pm \omega, \mathbf{K}_0 \pm \mathbf{K})$ . These currents give rise to electromagnetic–electrostatic side band modes at  $(\omega_0 \pm \omega, \mathbf{K}_0 \pm \mathbf{K})$ . The side-band modes in turn couple with the pump wave field  $\mathbf{E}_0(\omega_0, \mathbf{K}_0)$  to produce a ponderomotive force  $(\nabla \cdot (E^2))$  which drives and amplifies the density perturbation  $\delta n_j(K, \omega)$ . Thus a feed-back mechanism, schematically shown in Figure 5, is set up which leads to an instability in which the density perturbation  $\delta n_j(\omega, \mathbf{K})$  as well as the side band modes at  $(\omega_0 \pm \omega, \mathbf{K}_0 \pm \mathbf{K})$  both exponentiate with time.

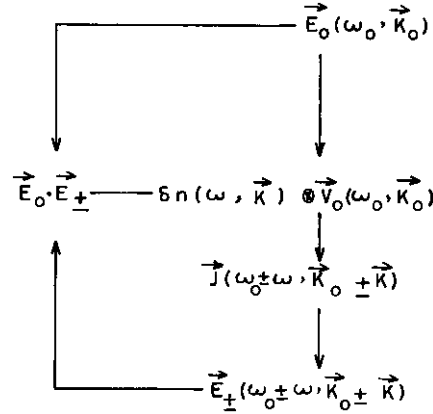


Figure 5. Feed back mechanism of parametric instabilities.

This description is valid to the first order in the fields of the two growing waves, provided the pump field  $\mathbf{E}_0(\omega_0, \mathbf{K}_0)$  exceeds a critical value.

The growth rate of the decay products for all the four processes discussed above can be derived using the equations of motion of the electrons and ions and Maxwell's equations. The Vlasov equation is then used to eliminate the first-order quantities in order to get the final dispersion relation from which growth rates of the various processes can be extracted under some simplifying assumptions. The equation of motion of the electrons and ions in the presence of a plane polarized pump field  $\mathbf{E}_0$  defined as

$$\mathbf{E}_0 = \frac{1}{2}[\mathbf{E}_{00}e^{i(\mathbf{K}_0 \cdot \mathbf{r} - \omega_0 t)} + \text{c.c}] \quad (4.5)$$

and the fields of the side band modes  $\mathbf{E}_+(\omega_0 + \omega, \mathbf{K}_0 + \mathbf{K})$  and  $\mathbf{E}_-(\omega_0 - \omega, \mathbf{K}_0 - \mathbf{K})$  can be written as

$$m_j \frac{d\mathbf{u}_j}{dt} = e_j [\mathbf{E}_0 + \mathbf{E}_+ + \mathbf{E}_-], \quad (4.6)$$

where the Lorentz force terms have been neglected as they are of the order of  $u_j/c \ll 1$ . Let us write

$$\mathbf{u}_j = \mathbf{u}_{0j} + \mathbf{u}_{+j} + \mathbf{u}_{-j}, \quad (4.7)$$

so that

$$\mathbf{u}_{0j} = \frac{ie_j \cdot \mathbf{E}_0}{m_j \omega_0}, \quad \mathbf{u}_{\pm j} = \frac{ie_j \mathbf{E}_{\pm}}{m_j \omega_{\pm}}, \quad (4.8)$$

where

$$\omega_{\pm} = \omega_0 \pm \omega.$$

Here  $\mathbf{u}_{0j}$  and  $\mathbf{E}_0$  are the zeroth-order quantities and  $\mathbf{u}_\pm$  and  $\mathbf{E}_\pm$  are the first-order quantities. Let us write the density  $n$  as

$$n = n_{0j} + \delta n_j(\mathbf{K}, \omega), \quad (4.9)$$

where, again  $n_{0j}$  is the zeroth-order density and  $\delta n_j$  is the first-order propagating density perturbation. One can now calculate the zeroth-order current  $\mathbf{J}_{0j}$  and the first-order current  $\mathbf{J}_{1j}$  from

$$\mathbf{J}_j = e_j [n_{0j} + \delta n_j(\mathbf{K}, \omega)] [\mathbf{u}_{0j} + \mathbf{u}_{+j} + \mathbf{u}_{-j}],$$

so that

$$\mathbf{J}_{0j} = e_j n_{0j} \mathbf{u}_{0j} \quad (4.10)$$

and

$$\mathbf{J}_{1j} = e_j n_{0j} [\mathbf{u}_{+j} + \mathbf{u}_{-j}] + e_j \delta n_j(\mathbf{K}, \omega) \mathbf{u}_{0j}.$$

Substituting from (4.8) for the  $u$ 's one finds the total current to the first order:

$$\mathbf{J}_{1j} = \frac{in_{0j}e_j^2\mathbf{E}_0}{m_j\omega_0} + \frac{in_{0j}e_j^2}{m_j} \left[ \frac{\mathbf{E}_+}{\omega_+} + \frac{\mathbf{E}_-}{\omega_-} \right] + \frac{ie_j^2\delta n_j(\mathbf{K}, \omega)\mathbf{E}_0}{m_j\omega_0}. \quad (4.11)$$

The wave equation derived from Maxwell's equations is given by

$$\left( \nabla^2 - \frac{1}{c^2} \frac{\partial^2}{\partial t^2} \right) \mathbf{E} = \nabla(\nabla \cdot \mathbf{E}) + \frac{4\pi}{c^2} \frac{\partial \mathbf{J}}{\partial t}, \quad (4.12)$$

where  $\mathbf{E}$  is the total electric field and  $\mathbf{J}$  is the total current due to all species of particles. Substituting (4.11) into (4.12), one finds, to the zeroth order

$$\left[ c^2 K_0^2 - \omega_0^2 + \sum_j \omega_{pj}^2 \right] \mathbf{E}_0 = c^2 \mathbf{K}_0 (\mathbf{K}_0 \cdot \mathbf{E}_0). \quad (4.13)$$

Since  $\mathbf{E}_0$  is a transverse electromagnetic field, the right-hand term of Equation (4.13) is zero and one gets the standard dispersion relation of an electromagnetic wave in a plasma, i.e.,

$$\omega_0^2 = \omega_{pe}^2 + \omega_{pi}^2 + K_0^2 c^2; \quad (4.14)$$

of course  $\omega_{pi} \ll \omega_{pe}$ .

From Equations (4.11) and (4.12), one gets to the first order:

$$D_+ \mathbf{E}_+ - c^2 \mathbf{K}_+ (\mathbf{K}_+ \cdot \mathbf{E}_+) + D_- \mathbf{E}_- - C^2 \mathbf{K}_- (\mathbf{K}_- \cdot \mathbf{E}_-) = \sum_j \frac{\omega_{pj}^2}{n_{0j}} n_j \mathbf{E}_{00} \times \left[ \frac{\omega_+}{\omega_0} e^{i(\mathbf{K}_+ \cdot \mathbf{r} - \omega_+ t)} + \frac{\omega_-}{\omega_0} e^{-i(\mathbf{K}_- \cdot \mathbf{r} - \omega_- t)} + \text{c.c.} \right], \quad (4.15)$$

where  $\delta n_j(\mathbf{K}, \omega) = \delta n_j e^{i(\mathbf{K} \cdot \mathbf{r} - \omega t)} + \text{c.c.}$

Equating the terms with common phase factors, we find:

$$D_{\pm} \mathbf{E}_{\pm} - c^2 \mathbf{K}_{\pm} (\mathbf{K}_{\pm} \cdot \mathbf{E}_{\pm}) = - \sum_j \frac{\omega_{pj}^2}{n_{0j}} \frac{\omega_{\pm}}{\omega_0} \delta n_j \mathbf{E}_{00}, \quad (4.16)$$

where

$$D_{\pm} = K_{\pm}^2 c^2 - \omega_{\pm}^2 + \sum_j \omega_{pj}^2. \quad (4.17)$$

In order to calculate the density fluctuation  $\delta n_j$  produced by the beating of the side-band modes with the pump field, we have to determine the force exerted by these waves on the plasma. This force is known as the ponderomotive force (Chen, 1974). This involves calculating the average rate of momentum transfer to the particles from the electromagnetic field. One notices that the average of the velocity calculated (Equation (4.8)) by neglecting the Lorentz force vanishes. In order to calculate the ponderomotive force, a higher-order calculation must be performed.

#### 4.2.1. The Ponderomotive Force

Radiation exerts pressure on matter. The plasma particles experience a nonlinear Lorentz force since the electric and magnetic fields are to be determined at the positions of the particles which move under the action of these fields. The Newton's equation of motion can be written as

$$m_j \frac{d\mathbf{V}_j}{dt} = e_j \left[ \mathbf{E}(\mathbf{r}) + \frac{\mathbf{V}_j}{c} \times \mathbf{B}(\mathbf{r}) \right]. \quad (4.18)$$

Let the velocity  $\mathbf{V}_j$  and the position vector  $\mathbf{r}$  of the particle be written as

$$\mathbf{r} = \mathbf{r}_0 + \mathbf{r}_1 + \mathbf{r}_2 + \dots, \quad \mathbf{V} = \mathbf{V}_0 + \mathbf{V}_1 + \mathbf{V}_2 + \dots. \quad (4.19)$$

Let  $\mathbf{E}(r) = E_s(\mathbf{r}) \cos \omega t$  be the electric field of the electromagnetic wave. Now to first-order, Equation (4.18) becomes

$$m_j \frac{d\mathbf{V}_{1j}}{dt} = e_j \mathbf{E}(\mathbf{r}_0),$$

so that

$$\mathbf{V}_{1j} = \frac{e_j \mathbf{E}_s(\mathbf{r}_0)}{m_j \omega} \sin \omega t. \quad (4.20)$$

Equation (4.20) is identical to Equation (4.8), since the electric field is determined at the undisturbed position  $r_0$  of the particle. Integrating (4.20), we find

$$\mathbf{r}_1 = -\frac{e_j \mathbf{E}_s(\mathbf{r}_0)}{m_j \omega^2} \cos \omega t. \quad (4.21)$$

The electric field  $\mathbf{E}(\mathbf{r})$  can be expanded about the equilibrium position  $\mathbf{r}_0$  as

$$\mathbf{E}(\mathbf{r}) = \mathbf{E}(\mathbf{r}_0) + (\mathbf{r}_1 \cdot \nabla) \mathbf{E}_s(\mathbf{r})|_{r=r_0} + \dots \quad (4.22)$$

and the corresponding magnetic field  $\mathbf{B}(r)$  is found to be

$$\mathbf{B}(\mathbf{r}) = -\frac{c}{\omega} \nabla \times \mathbf{E}_s(r) \sin \omega t. \quad (4.23)$$

Now Equation (4.18) to second order gives

$$m_j \frac{d\mathbf{V}_{2j}}{dt} = e_j \left[ (\mathbf{r}_1 \cdot \nabla) \mathbf{E}_s(\mathbf{r})|_{r=r_0} + \frac{\mathbf{V}_{1j}}{c} \times \mathbf{B}(\mathbf{r}) \right]. \quad (4.24)$$

One notices that there are two sources of nonlinearity, one due to determining the electric field at the displaced position of the particle and other due to the magnetic field of the wave. Substituting for  $\mathbf{r}_1$ ,  $\mathbf{V}_{1j}$ , and  $\mathbf{B}(r_0)$ , we find

$$m_j \frac{dV_{2j}}{dt} = -\frac{e_j^2}{m_j \omega^2} [(\mathbf{E}_s(r_0) \cdot \nabla) \mathbf{E}_s(r_0) \cos^2 \omega t + \mathbf{E}_s(\mathbf{r}_0) \times \nabla \times \mathbf{E}_s(r_0) \sin^2 \omega t].$$

Taking the average over the period  $t = 2\pi/\omega$ , we find

$$m_j \left\langle \frac{dV_{2j}}{dt} \right\rangle = -\frac{e_j^2}{4m_j \omega^2} [\nabla E_s^2(r_0)] = f_{NL}. \quad (4.25)$$

Thus the nonlinear force  $f_{NL}$  on a single particle has been found. The total force per  $\text{cm}^3$  is given by

$$\mathbf{F}_{NL} = \sum_j n_{0j} f_{NL} = \sum_j -\frac{\omega_{pj}^2}{8\pi\omega^2} \nabla \langle E^2(r_0) \rangle. \quad (4.26)$$

Since

$$\langle E^2(r) \rangle = \frac{E_s^2(r)}{2}.$$

Writing  $\mathbf{F}_{NL} = -\nabla\Psi$  one finds the ponderomotive potential on particles of  $j$ th species as

$$\Psi_j = \frac{\omega_{pj}^2}{\omega^2} \frac{E^2(r_0)}{8\pi}. \quad (4.27)$$

In the presence of the pump field  $\mathbf{E}_0$  and the side band fields  $\mathbf{E}_\pm$ , to the first order in  $\mathbf{E}_\pm$ , the potential  $\psi_j$  can be generalized to

$$\Psi_j = \frac{n_{0j}e_j^2}{m_j\omega_0^2} [\mathbf{E}_0 \cdot \mathbf{E}_- + \mathbf{E}_0 \cdot \mathbf{E}_+]. \quad (4.28)$$

The force on a single particle is  $\mathbf{F}_j = -\nabla\psi_j/n_j = -\nabla\psi_j$ .

#### 4.2.2. Dispersion Relation

Once the driving potential due to the three electromagnetic waves  $E_0, E_\pm$  has been determined, the density perturbation  $\delta n_j$  can be determined from the Vlasov equation:

$$\frac{\partial f_j}{\partial t} + \mathbf{V} \cdot \nabla f_j + \frac{1}{m_j} [-e_j \nabla \varphi - \nabla \psi_j] \frac{\partial f_j}{\partial \mathbf{V}} = 0, \quad (4.29)$$

where  $f_j(\mathbf{r}, \mathbf{V}, t)$  is the particle distribution function and  $\varphi$  is the electrostatic scalar potential associated with electrostatic waves. Thus,  $[-e_j \nabla \varphi - \nabla \psi_j]$  is the total force due to electrostatic and electromagnetic waves on a single particle. Using the standard techniques of linearizing Equation (4.29) and Fourier analysing all the first-order quantities ( $f_{j1}, \varphi, \psi_j$ ) we find:

$$f_{j1} = \frac{1}{m_j} [-e_j \varphi - \psi_j] \mathbf{K} \frac{\partial f_{0j}}{\partial \mathbf{V}} \frac{1}{(\omega - \mathbf{K} \cdot \mathbf{V})} \quad (4.30)$$

and

$$\delta n_j(\mathbf{K}, \omega) = \int_{-\infty}^{\infty} n_{0j} f_{j1} d^3V = \frac{k^2}{4\pi e_j^2} [-e_j \varphi - \psi_j] \chi_j, \quad (4.31)$$

where

$$\chi_j(\mathbf{K}, \omega) = \frac{\omega_{pj}^2}{K^2} \int_{-\infty}^{\infty} \mathbf{K} \cdot \frac{\partial f_{0j}}{\partial \mathbf{V}} \frac{d^3V}{(\omega - \mathbf{K} \cdot \mathbf{V})} \quad (4.32)$$

is the particle susceptibility function. For a Maxwellian plasma

$$f_{0j} = \left( \frac{m_j}{2\pi K_B T_j} \right)^{3/2} \exp[-V^2/V_j^2], \quad (4.33)$$

one finds

$$\chi_j(\mathbf{K}, \omega) = \frac{1}{(K\lambda_{Dj})^2} \left[ 1 + \frac{\omega}{KV_j} Z(\omega/KV_j) \right], \quad (4.34)$$

where  $Z(\zeta)$  is the plasma dispersion function (Fried and Conte, 1961) defined as

$$Z(\zeta) = \frac{1}{\sqrt{\pi}} \int_{-\infty}^{\infty} \frac{e^{-x^2} dx}{(x - \zeta)},$$

$V_j = (2K_B T_j/m_j)^{1/2}$  is the thermal velocity and  $\lambda_{Dj} = (T_j/4\pi n_{0j} e_j^2)^{1/2}$  is the Debye wavelength. The asymptotic forms of the susceptibilities  $\chi_j$  are found to be:

$$\begin{aligned} \chi_j(K, \omega) &= -\frac{\omega_{pj}^2}{\omega^2} \left( 1 + \frac{3}{2} \frac{K^2 V_j^2}{\omega^2} \right) + \frac{i\sqrt{\pi}}{(K\lambda_{Dj})^2} \left( \frac{\omega}{KV_j} \right) \times \\ &\quad \times \exp[-\omega^2/(KV_j)^2] \quad \text{for } \omega \gg KV_j \\ &= \frac{1}{(K\lambda_{Dj})^2} \left[ 1 + i\sqrt{\pi} \frac{\omega}{KV_j} \right] \quad \text{for } \omega \ll KV_j. \end{aligned} \quad (4.35)$$

The electrostatic potential  $\varphi$  is related to the density perturbation  $\delta n_j$  through the Poisson equation:

$$\nabla^2 \varphi = -4\pi \sum_j (e_j n_j), \quad (4.36)$$

or in the Fourier transformed form

$$\varphi(\mathbf{K}, \omega) = \frac{4\pi}{K^2} \sum_j e_j \delta n_j, \quad (4.37)$$

since  $n_{0e} = n_{0i}$ . Substituting for  $\delta n_j$  from Equation (4.31), one finds

$$\varphi(\mathbf{K}, \omega) = \frac{1}{\epsilon} \sum_j -\frac{\psi_j \chi_j}{e_j}, \quad (4.38)$$

where  $\epsilon = 1 + \sum_j \chi_j(\mathbf{K}, \omega)$  is the plasma dielectric function. Substituting Equation (4.38) into (4.31) and using Equation (4.28), we find:

$$\delta n_j = \frac{K^2}{4\pi e_j^2 \omega_0^2} \left[ \frac{e_j}{\epsilon} \sum_{j'} \frac{e_{j'} \chi_{j'}}{m_{j'}} - \frac{e_j^2}{m_j} \right] \chi_j \times (\mathbf{E}_0 \cdot \mathbf{E}_- + \mathbf{E}_0 \cdot \mathbf{E}_+). \quad (4.39)$$

Combining Equations (4.16) and (4.39) we can eliminate the first-order perturbation  $\delta n_j$  to get the linear dispersion relation

$$\begin{aligned} 1 = & \sum_j \frac{\omega_{pj}^2 K^2 \chi_j}{4\pi e_j^2 n_0 \omega_0^2} \left[ \frac{e_j}{\epsilon} \sum_{j'} \frac{e_{j'}}{m_{j'}} + \frac{e_j^2}{m_j} \right] \times \\ & \times \left[ \frac{(\vec{\mathbf{K}}_+ \times \mathbf{E}_0)^2 \omega_+}{D_+ K_+^2 \omega_0} + \frac{(\mathbf{K}_+ \cdot \mathbf{E}_0)^2 \omega_+}{K_+^2 (D_+ - c^2 K_+^2) \omega_0} \right] + \\ & + \left[ \frac{(\vec{\mathbf{K}}_- \times \mathbf{E}_0)^2 \omega_-}{D_- K_-^2 \omega_0} + \frac{(K_- \cdot E_0)^2 \omega_-}{K_-^2 (D_- - c^2 K_-^2) \omega_0} \right]. \end{aligned} \quad (4.40)$$

The dispersion relation was derived by Liu and Kaw (1976) where they retained only the  $j = e$  term and also used the approximation  $\omega_{pe}^2 \gg \omega_{pi}^2$  and  $(\omega + \omega_0) \simeq (\omega_- / \omega_0) \simeq 1$ . Equation (4.40) is the exact dispersion relation where electrons and ions have been treated on par. The four cases of instabilities discussed earlier can be studied using Equation (4.40).

## 5. The Parametric Decay Instability in Quasars

As discussed in the Introduction the line-emitting region of a quasar is in the form of gas clouds which are irradiated by the nonthermal continuum radiation of the central source. In addition to the photoionization and heating of the emission line regions of quasars by the high-frequency radiation, microwave heating and ionization can also occur. From the constraints imposed by the observations of the emission lines, it has been concluded that a range of electron densities and temperatures exist in these regions. One can ascertain by checking the conditions for an ionized medium to behave like a plasma that the emission line regions (ELR) with electron density  $n_e \sim 10^8 - 10^{12} \text{ cm}^{-3}$  and temperature at  $T \sim 10^4 - 10^5 \text{ K}$  is a plasma. It is expected that surrounding the relatively cool photoionized regions, lie the rarer and the hotter regions and additional heating mechanisms may be required to maintain them. Davidson and Netzer (1979) have reviewed some of the additional heating mechanisms. Osterbrock and Parker (1965) and Eilek and Caroff (1976) proposed that energetic nonthermal charged particles could cause excitations and heating. Nussbaumer and Osterbrock (1970) have held cloud-cloud collisions to be responsible for producing ionizing radiation. Dattabuit and Cox (1972), Dattabuit et al. (1978) and Davidson (1972) have considered several consequences of the cloud-cloud collisions like shocks, compression and heating. Krolik et al. (1978)

pointed out that radio frequency waves can heat the gas through free-free absorption processes.

The electron densities of the thermal plasma in the environs of a quasar are such that the corresponding electron-plasma frequencies lie in the range of radio frequencies. This opens up several avenues by which the radio radiation can be absorbed in the ELR plasma or in the accretion disc plasma by processes more efficient than the collisional. Through the processes of the parametric decay instability and the stimulated Raman, Brillouin, and Compton scattering followed by the damping of the electron plasma and the ion-acoustic waves, the plasma can be heated to much higher temperatures in much shorter times. These absorption processes also modify the spectral distribution of the radio radiation. The bends in the radio continuum of a quasar could, therefore, be in part accounted for by the plasma absorption processes.

In order to quantitatively study the plasma radiation coupling processes, one has to analyse the dispersion relation Equation (4.40). One looks for complex roots for frequency  $\omega$  for real wavevector  $\mathbf{K}$ . One way to locate complex roots is to look for conditions under which one of the denominators of Equation (4.40) nearly vanishes. One observes that Equation (4.40) has two types of denominators  $D_+$  or  $D_-$  and  $D_+ - c^2 K_\pm^2$  or  $(D_- - c^2 K_-^2)$ . The four processes of plasma radiation coupling correspond to near vanishing of one or the other of these denominators. Thus, PDI ensues when  $(D_- - c^2 K_-^2) \simeq 0$  or  $\omega_- = \omega_0 - \omega \simeq \omega_{pe}$ . The electromagnetic wave  $(\omega_0 \mathbf{K}_0)$  decays to an electron plasma wave  $\omega_- \equiv \omega_e$  and another low-frequency electrostatic wave,  $\omega \equiv \omega_i$ , the ion-acoustic wave. The momentum conservation condition  $\mathbf{K}_- = \mathbf{K}_0 - \mathbf{K}$  gives  $\mathbf{K}_- \equiv \mathbf{K}_e \simeq -\mathbf{K} \equiv \mathbf{K}_i$  since for  $\omega_0 \simeq \omega_{pe}$ ,  $K_0 \simeq 0$ . The PDI can be studied by retaining only terms (2) and (4) in Equation (4.40); using the asymptotic forms of susceptibilities in the regime  $KV_e \gg \omega \simeq KV_i$ ; replacing  $\omega_-$  by  $\omega_- - i\Gamma_e$  in order to include the damping  $\Gamma_e$  of the electron plasma wave  $\omega_-$  and making use of the approximations valid for this case (like  $\omega_0 \simeq \omega_{pe}$ ,  $\omega \ll \omega_0$ , etc.), one finds the growth rate or the imaginary part of  $\omega$  of the exponentially growing waves  $\omega_-$  and  $\omega$  to be

$$\gamma = \frac{(\mathbf{K} \cdot \mathbf{V}_0)^2 \omega_{pi}^2}{KC_s \omega_{pe} \Gamma_i} - \Gamma_e, \quad (5.1)$$

where

$$V_0 = \frac{eE_0}{m_e \omega_0}, \quad \Gamma_e = \frac{\sqrt{\pi} \omega_{pe}}{2K^3 \lambda_{De}^3} \exp \left[ -\frac{1}{2K^2 \lambda_{De}^2} - \frac{3}{4} \right] + \nu_{ei},$$

the electron-ion collision frequency  $\nu_{ei} \simeq 50n_0 T^{-3/2} \text{ s}^{-1}$  and the ion wave damping rate  $\Gamma_i$  is

$$\Gamma_i = \sqrt{\frac{\pi}{8}} KC_s \left( \frac{m_e}{m_i} \right)^{1/2} \left( \frac{T_e}{T_i} \right)^{3/2} \exp \left[ -\frac{1}{2} \left( 3 + \frac{T_e}{T_i} \right) \right]. \quad (5.2)$$

Since the electron-plasma wave and the ion-acoustic wave suffer damping, the amplitude of the pump wave must be large enough so that the growth rate exceeds the damping rate. This gives a threshold field  $E_{DT}$  for which the growth rate is zero as

$$\frac{(K \cdot V_{0T})^2}{4K C_s} \omega_{pi} \sqrt{\frac{m_e}{m_i}} = \Gamma_e \Gamma_i, \quad (5.3)$$

where

$$V_{0T} = \frac{eE_{0T}}{m_e \omega_0}.$$

Equation (5.3) describes the minimum value of the electric field  $E_0$  required such that the rate at which the energy is being fed into the electron plasma and the ion-acoustic waves equals their damping rate. Equation (5.1) gives the growth rate just above the threshold. After an initial period of exponential growth, the electrons and ions begin to heat up due to the absorption of the electrostatic waves, consequently the damping increases, and conditions close to the threshold (Equation (5.3)) obtain. The instability shuts off. The maximum damping rate can be estimated again from Equation (5.3) from which one sees that the electron and ion temperature become function of the electric field of the pump electromagnetic field. Thus the maximum effective damping rate  $\Gamma_{\text{eff}}^2$  is given by

$$\Gamma_{\text{eff}}^2 = \frac{(K \cdot V_0)^2}{4K C_s} \omega_{pi} \sqrt{m_e m_i}. \quad (5.4)$$

### 5.1. INCOHERENCE OF THE INCIDENT FIELD

The above results have been derived assuming the incident field to be a perfectly coherent field. In reality, some amount of incoherence is always present. It has been shown by Tamor (1973) and Thomson et al. (1974) that the effects of finite bandwidth  $\Delta\omega_0$  of the incident field on the parametric instabilities can be taken care of by replacing the damping rate  $\Gamma_e$  of the waves by  $(\Gamma_e + 2\xi) \sim (\Gamma_e + \Delta\omega_0)$  where  $\xi$  is the number of phase jumps per unit time. This is so because  $\Gamma_e$  is a measure of the duration of time an electron is allowed to oscillate with the driving field before being knocked out of phase by a collision. The same effect results when the driving field suffers a phase shift. Thus the two effects are additive. Replacing  $\Gamma_e$  by  $(\Gamma_e + \Delta\omega_0)$  raises the threshold for the instability and the effective damping rate (Equation (5.4)) is modified to

$$\Gamma_{\text{eff}}^2 = \frac{(K V_0)^2}{4K C_s} \omega_{pi} \sqrt{\frac{m_e}{m_i}} \frac{1}{(1 + \Delta\omega_0/\Gamma_e)}. \quad (5.5)$$

Another source of the incoherence of the pump radiation is the lack of definite polarization. In an unpolarized beam, the tip of the electric vector undergoes random changes of direction. Thus an electron in such a field undergoes changes in its direction of motion at the same rate. This further increases the rate of collisions and hence the threshold. If, for example the incident radiation has 10% polarization, only 10% of the total luminosity is actually available for driving the instability. Also, as the instability sets up, plasma temperatures  $T_e$  and  $T_i$  go up due to the damping of excited electrostatic waves and so do  $\omega_e$  and  $\omega_i$ . Since  $\omega_0 = \omega_e + \omega_i$ , the resonant pump frequency  $\omega_0$  should also increase. Therefore a band of pump frequencies can satisfy the resonance condition. An inhomogeneity in plasma density will also admit a broad pump. Under the circumstances where the resonant condition is satisfied for the entire band-width  $\Delta\omega \simeq \omega_0$ , the growth rate  $\gamma_1 = \gamma_1^2/\Delta\omega$  where  $\gamma_1$  is the growth rate due to a monochromatic pump (Kruer, 1988).

## 5.2. HEATING OF EMISSION LINE REGIONS

From the emission line properties of AGN, a large range of densities and temperatures has been inferred for the clouds of the ELR. The intense radiation emitted from the central region is also of a broad band. And the question arises if this broad band radiation can be absorbed in ELR through the parametric decay instability. It is conceivable that the incident radiation of a particular frequency  $\omega_0$  will excite PDI in a plasma cloud of the density such that the resonance condition is satisfied. This way, different spectral portions of the incident radiation get absorbed in clouds of different densities. For example if the electron density  $n_0$  varies, say, from  $10^8 - 10^{13} \text{ cm}^{-3}$  then radio radiation in the frequency range  $\omega_0 \sim 5.5 \times 10^4 \sqrt{n_0}$  will get absorbed through PDI. Now, the electric field  $E_0$  can be determined by using the relation  $E_0^2 = L/R^2 C$  where  $L$  is the luminosity of the radio radiation and  $R$  is the distance of the cloud from the source of radio radiation. It is found that the maximum absorption rate  $\text{cm}^{-1}$ :

$$\frac{\Gamma_{\text{eff}}}{c} \simeq 2 \times 10^{-5} \left( \frac{L_{41} K \lambda_{\text{De}}}{r_{pc}^2 T_4} \right)^{1/2} \text{ cm}^{-1}, \quad (5.6)$$

which is much larger than the free-free absorption rate  $\nu_{ei}/c \simeq 1.4 \times 10^{-7} n_8 T_4^{-3/2} \text{ cm}^{-1}$  for typical values of the parameters, where  $L = L_{41} \times 10^{41} \text{ erg s}^{-1}$ , etc. In fact, in some sources  $L_{41} \gg 1$ . By substituting for  $\Gamma_{\text{eff}}^2 = \Gamma_e \Gamma_i$ , one can estimate the value of  $(K \lambda_{\text{De}})_{\text{max}}$  and hence the final temperature of the plasma (Krishan, 1987). It is found that the electron temperature can increase by an order of magnitude even for moderate radio luminosities of  $\sim 10^{41} \text{ erg s}^{-1}$ . The parametric decay instability may also provide a mechanism for the formation of hot lower density corona adjoining each photoionized dense region. This process is also likely to be operating in the BL Lacertae objects where the absence of dense gas clouds is attributed to the strong radio frequency heating (Krolik et al., 1978). In

addition, the low-frequency turnover attributed to synchrotron self-absorption in an inhomogeneous multicomponent source is a commonly observed feature. The anomalous absorption in this region may also produce spectral modifications.

### 5.3. 21-CM ABSORPTION

The standard interpretation of the 21-cm absorption observed in several QSO systems is that it originates in the neutral hydrogen clouds lying along the line of sight (Weymann et al., 1981). The 21-cm radiation absorption is conventionally associated with the spin-flip transition of neutral hydrogen atoms. The absorption rate for the spin-flip transition is given as

$$K(\omega) = 2.58 \times 10^{-15} \frac{f(\omega)N}{T_K} \text{cm}^{-1}, \quad (5.7)$$

where,  $T_K$  is the temperature which characterises the population distribution between the two atomic states,  $f(\omega)$  is the line-shape function normalized to unity and  $N$  is the number of hydrogen atoms  $\text{cm}^{-3}$ .

The process of PDI provides another mode for the absorption of 21-cm radiation. Through this process, 21 cm (1420 MHz) radiation can be absorbed in a plasma of electron-plasma frequency of 1420 MHz. The emission line regions have the right range of electron densities to provide such a plasma. One can check that the absorption rate for the parametric decay process (Equation (5.6)) is much larger than that for the spin-flip transition for the standard values of the parameters. Absorption of radio radiation by parametric decay certainly has a line character since only that spectral portion which satisfies the resonance conditions, gets absorbed. Thus, the plasma, depending upon its electron density, picks up the electromagnetic radiation of the right frequency. The width of the absorption feature may be due to the width of the electron density variation in the plasma (Krishan, 1988a). But, as is inferred from emission-line studies, if the region has a range of electron densities, the absorption from each region will be superimposed and the profile may be broadened beyond recognition.

Since, the PDI is a collective process, the absorption rate of the radio radiation around 21-cm is extremely high. As a result, the effective absorption occurs over much shorter path lengths in the line of sight. This has implications for the shape of the absorbing plasma. The neutral hydrogen clouds are much farther from the source of the continuum 21-cm radiation than is the emission line region. Therefore 21-cm radiation will be first intercepted by the emission line region and can undergo strong absorption through PDI. The radio emitting region, being of large size, may overlap a significant portion of the emission line region. The radiation that leaks through is available to be absorbed in neutral hydrogen regions. Thus, in conclusion, since the conditions for the parametric decay process to occur are satisfied, absorption of 21-cm radiation will take place in the emission line region. If so, then absorption of 21-cm radiation cannot be attributed entirely to neutral hydrogen.

#### 5.4. VARIANTS OF PDI

A very intense incident radiation begins to modify the normal modes of the plasma. The frequencies of these modes become functions of the incident radiation. Thus, for large strength of the incident radiation and at low temperatures, the ion mode loses its linearity. This mode is now known as the Reactive Quasi-Ion Mode and its frequency and growth rate are much larger than the ion-acoustic wave frequency ( $\omega_i = K c_s$ ).

For electron temperature  $T_e < T_i$ , the ion temperature, the ion mode is strongly damped due to nonlinear Landau damping over the thermal ions. In this case compared to other cases, a weak instability is excited and the process is known as decay into a Resistive Quasi-Ion Mode.

When an intense radiation of frequency less than the frequency of an electron plasma wave ( $\omega_{pe} < \omega_0 < \omega_e$ ) is incident it couples with a high-frequency wave ( $\omega_e, \mathbf{K}_e$ ) and a non-oscillatory ion mode ( $0, \mathbf{K}_i$ ). In this case, the thermal ion density fluctuations of zero-frequency grow along with the electron plasma wave. Since, these static density fluctuations do not qualify as a wave, this instability, known as the oscillating two stream instability, is sometimes not included in the class of parametric instabilities.

A detailed account of these cases of PDI has been given in Gangadhara and Krishan (1990). The variation of growth rates with electron temperature  $T_e$  using typical values of various parameters for the source 3C273 is presented in Figure 6. Here  $\nu_0 = (\omega_{pe}/\omega_0)^2$  is the collisional damping rate of the electromagnetic wave;  $\gamma_1, \gamma_2, \gamma_3$ , and  $\gamma_{OTS}$  are the growth rates of the PDI, the reactive quasi-ion mode, the resistive quasi-ion mode and the oscillating two-stream instability.

The parametric decay instability is a much faster process compared to all other processes of absorption. The excited electron-plasma wave undergoes Landau damping and heats the plasma. In addition, other processes such as two-electron plasma waves combine to give an electromagnetic wave, which can undergo PDI. Thus, the incident radiation could be either totally absorbed and or suffer a spectral change. These processes have a tremendous diagnostic potential and need to be investigated in a variety of intense astrophysical sources.

### 6. Stimulated Raman and Compton Scattering in Quasars

There are three ways by which the scattering of radiation in a plasma can occur: (i) stimulated Raman scattering (SRS), where a strong electromagnetic wave is scattered off a weakly damped electron plasma wave ( $K_e \lambda_{De} \ll 1$ ), (ii) stimulated Compton scattering (SCS), where a strong electromagnetic wave is scattered off a highly damped electron plasma wave ( $K_e \lambda_{De} \gtrsim 1$ ), and (iii) Compton or the Thomson scattering (CS), where the electromagnetic radiation is scattered by single electrons (Figure 7). Although the stimulated scattering processes are well known

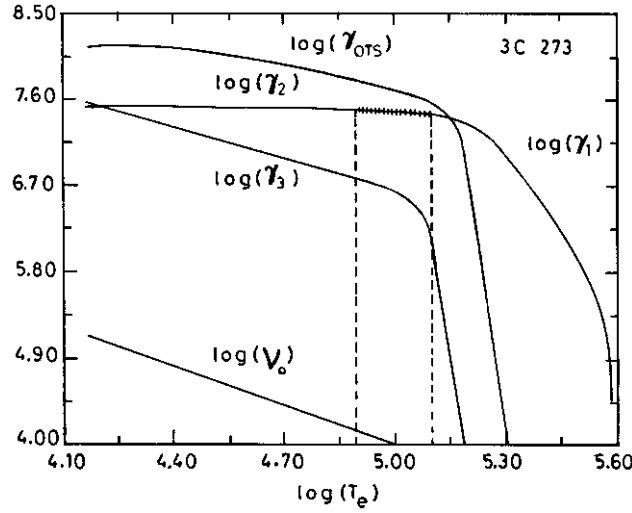


Figure 6. Variation of growth rates  $\gamma_j$  vs electron temperature  $T_e$  for an incident wave of frequency  $\omega_0 = 1.01\omega_{pe}$  for plasma parameters of the source 3C273,  $j = 1$ , for the PDI;  $j = 2$ , for the reactive quasi-ion mode;  $j = 3$ , for the resistive quasi-ion mode and  $\gamma_{OTS}$  is for the oscillating two-stream instability.

among laboratory plasma physicists, they remained unknown to astrophysicists until the work of Krishan (1983). Under appropriate conditions, these plasma processes play a decisive role in the generation as well as the reprocessing of electromagnetic radiation. In addition, the plasma gets heated due to the damping of the electron plasma wave. The decay of a large amplitude electromagnetic wave ( $\omega_0, \mathbf{K}_0, \vec{\mathbf{E}}_0$ ) into another electromagnetic wave ( $\omega_s, \mathbf{K}_s, \mathbf{E}_s$ ) and an electron plasma wave ( $\omega_e, \mathbf{K}_e, \mathbf{E}_p$ ) occurs when the phase matching conditions  $\omega_0 = \omega_s + \omega_e$  and  $\mathbf{K}_0 = \mathbf{K}_s + \mathbf{K}_e$  are satisfied. One can check that the denominator

$$D_-(\mathbf{K}_-, \omega_-) = K_-^2 c^2 - \omega_-^2 + \omega_{pe}^2 \simeq 0 \quad \text{for} \quad K_e \simeq 2K_0 \cos \theta_e,$$

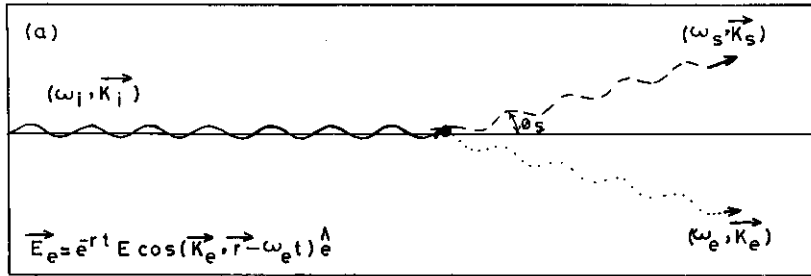
where  $\cos \theta_e = \mathbf{K}_e \cdot \mathbf{K}_0 / |K_e| |K_0|$  (Equation (4.40)). The scattering angle  $\theta_s$  is given by  $\cos \theta_s = 1 - 2 \cos^2 \theta_e$ . Thus  $\theta_e = 0$  or  $\theta_s = \pi$  corresponds to backscattering. The growth rate of the exponentially growing waves  $\omega_- \equiv \omega_s$  and  $\omega_e$  can be determined from the dispersion relation Equation (4.40) under various approximations. Including the damping terms for the electron plasma wave  $\Gamma_e$  and the scattered electromagnetic wave  $\Gamma_s$  as before, one finds the maximum growth rate for stimulated Raman Scattering  $\gamma_{SRS}$  to be:

$$\gamma_{SRS} = \frac{V_0}{c} (\omega_{pe} \omega_0)^{1/2} \psi \quad \text{for} \quad \omega_{pe} > \gamma_{SRS} > \Gamma_e, \quad (6.1)$$

where  $\psi = \cos \theta_e |\sin \varphi|$  and  $\varphi = \pi/2$ , when the incident and the scattered waves are polarized in the same direction.

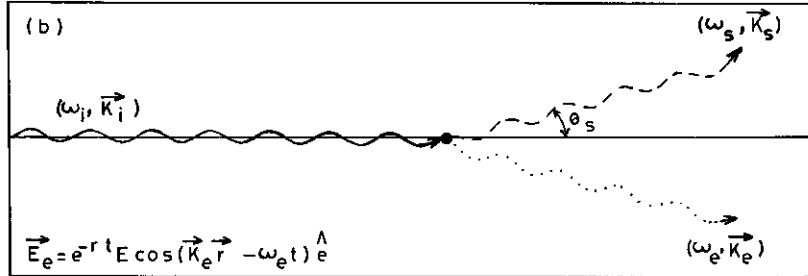
The threshold for SRS (backscattering) is given by

STIMULATED RAMAN SCATTERING ( $k_e \lambda_{De} \ll 1$ )



$\vec{E}_s$  is the electric field of a weakly damped electron plasma wave

STIMULATED COMPTON SCATTERING ( $k_e \lambda_{De} \geq 1$ )



$\vec{E}_e$  is the electric field of a strongly damped electron plasma wave

COMPTON SCATTERING

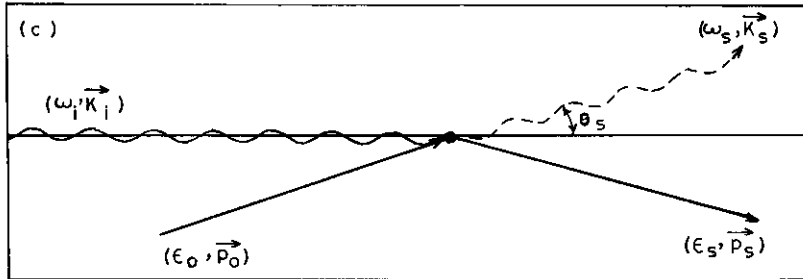


Figure 7. The three modes of scattering of an electromagnetic wave in a plasma.

$$\left(\frac{V_{0t}}{c}\right)^2 = \frac{1}{\psi^2} \left(\frac{\Gamma_e}{\omega_{pe}}\right) \left(\frac{\Gamma_s}{\omega_s}\right), \quad (6.2)$$

where

$$\Gamma_s = \nu_{ei} \frac{\omega_{pe}^2}{2\omega_s^2}$$

is the collisional damping rate of the scattered wave.

Stimulated Raman scattering changes to stimulated Compton scattering when the electron plasma wave is heavily damped, i.e., for  $K_e \lambda_{De} \gg 1$ . The threshold for SCS is given by

$$\left(\frac{V_{0t}}{c}\right)^2 = 2 \left(\frac{2}{\pi}\right)^{1/2} \left(\frac{\Gamma_s}{\omega_0}\right) (K_0 \lambda_{De})^2 \exp\left(\frac{1}{2}\right) \quad (6.3)$$

and the growth rate  $\gamma_{SCS}$  is found to be

$$\gamma_{SCS} = \frac{\omega_0 V_0^2 \sqrt{\pi}}{2 c^2} (K_0 \lambda_{De})^{-2} \exp\left(-\frac{1}{2}\right) - \Gamma_s . \quad (6.4)$$

Below a few examples of the role of these processes in quasars are presented.

### 6.1. HEATING OF THE INTERCLOUD MEDIUM

The broad emission line regions of quasars consist of high electron density ( $n = 10^{10}-10^{11} \text{ cm}^{-3}$ ) and low temperature ( $T \sim 10^4-10^5 \text{ K}$ ) clouds probably confined by a low-density ( $n \simeq 10^4 \text{ cm}^{-3}$ ) and high-temperature ( $T \sim 10^8-10^9 \text{ K}$ ) intercloud medium. The intercloud medium is heated to such temperatures by Compton scattering of high-frequency non-thermal radiation of the quasar (Levich and Sunyaev, 1971). If Compton heating is the main mechanism, then the clouds can be in pressure equilibrium with the intercloud medium over a small range of pressures in the neighbourhood of  $(nT) \sim 10^{12}-10^{14} \text{ K cm}^{-3}$ . The need for additional heating processes is evident. First, the range of equilibrium pressures need to be extended. Second, the intercloud medium exerts a drag force on the moving clouds and the drag limited speed is found to be too small for  $T \sim 10^8 \text{ K}$  to account for the observed line-widths. Third, a higher intercloud temperature can lead to a simpler motion of the clouds, as is indicated by the uniformity and simplicity of the line profiles observed in quasars and Seyferts. These points have been discussed by Mathews and Capriotti (1985). Additional heating by cloud motions and cosmic rays has been suggested by Mathews (1974) and Krolik et al. (1981). The contribution of SRS and SCS to the heating of the intercloud medium was pointed out first by Krishan (1988b). It was shown that the threshold conditions for SRS and SCS are satisfied for the typical parameters of a quasar and its intercloud medium. The threshold condition (Equation (6.2)) for SRS translate to

$$\left(\frac{L_{47}}{r_{pc}^2}\right)_{\text{SRS}} \gtrsim \frac{2.85 \times 10^{-4} n_4^{1/2}}{T_8^3} \left[ \frac{26.7 \times 10^{14} n_4^3}{\omega_0^3} \times \right. \\ \left. \times \exp\left(-\frac{1.2 \times 10^{18} n_4}{\omega_0^2 T_8} - \frac{3}{4}\right) + 2.3 \times 10^{-14} n_4^2 \right] , \quad (6.5)$$

where, the symbols have their usual meaning. The condition  $K_e \lambda_{De} \ll 1$  and  $\omega_0 \simeq K_0 c \gg \omega_{pe}$  translates to

$$5.46 \times 10^6 n_4^{1/2} \ll \omega_0 \ll 1.54 \times 10^9 n_4^{1/2} T_8^{-1/2}, \quad (6.6)$$

for  $\cos \theta_e \simeq 10^{-2}$ , i.e., for nearly forward scattering. One must realize that the inequality in Equation (6.5) drives the SRS. At a higher value of  $T_8$ , the SRS stops and the plasma and radiation are said to be in equilibrium.

The threshold condition for SCS (Equation (6.3)) translates to

$$\left( \frac{L_{47}}{r_{pc}^2} \right)_{\text{SCS}} \geq 6 \times 10^{-23} \omega_0 n_4 T_8^{-1/2} \quad (6.7)$$

and the condition  $K_e \lambda_{De} \gg 1$  translates to

$$\omega_0 \gg \frac{1.54 \times 10^7}{\cos \theta_e} n_4^{1/2} T_8^{1/2}. \quad (6.8)$$

It is found that the growth rate  $\gamma_{\text{SCS}}$  is much smaller than  $\gamma_{\text{SRS}}$  but it is still much larger than  $\gamma_c$  which is the scattering rate when the isotropic radiation is scattered by individual electrons. In conclusion, depending upon the frequency and the energy density of the incident radiation and the electron density and the temperature of the plasma, one or more of the three scattering processes may occur. Through SRS and SCS, the nonthermal radio radiation equilibrates with the intercloud medium at much higher temperatures than are achievable through single particle Compton scattering.

## 6.2. REPROCESSING OF THE SYNCHROTRON SELF-ABSORBED RADIATION

The discrepancies between the observed flat spectrum (typically  $\alpha \simeq 0.03$ – $0.3$  with  $F_\nu \propto \nu^{-\alpha}$ ) of the compact extragalactic sources at low frequencies and the predictions of the homogeneous synchrotron model in the self-absorbed part of the spectrum ( $F_\nu \propto \nu^{5/2}$ ) are usually explained by invoking multiple components, inhomogeneity and/or specialized spectra of the energetic electrons (Spangler, 1982). The stimulated Raman scattering of the self-absorbed radiation in the accretion disc plasma can reprocess the radiation to produce a flat spectrum (Krishan, 1988c).

Equal amounts of energy go to the scattered electromagnetic radiation and the electron plasma wave for  $\omega_0 = 2\omega_e$ , as dictated by the Manley–Rowe relations for conservation of wave action (Figueroa et al., 1984). The energy density of the electron plasma wave can be estimated by invoking a saturation mechanism of the SRS instability. When the amplitude of the electron plasma wave  $E_e$  grows large enough to trap electrons in its field and therefore increase the effective electron thermal speed, the electron-plasma wave is Landau-damped and SRS stops. The saturation is reached when the growth rate of SRS is equal to the damping rate of the electron-plasma wave (Hasegawa, 1978; Krishan, 1983), i.e.,

$$\gamma_{\text{SRS}} = \Gamma_e(E_e^2) = \frac{\sqrt{\pi}\omega_{pe}}{2K_e^3\lambda_{\text{D eff}}^3} \exp\left[-\frac{1}{2K_e^2\lambda_{\text{D eff}}^2} - \frac{3}{4}\right], \quad (6.9)$$

$$\lambda_{\text{D eff}} = \frac{V_{\text{eff}}}{\omega_{pe}}; \quad V_{\text{eff}} = \left(\frac{2eE_e}{m_e K_e}\right)^{1/2}$$

and  $K_e = 2K_0$  for backscattering. From Equation (6.9), the energy density of the electron plasma wave, which is also the energy density  $E_s^2$  of the scattered electromagnetic wave is found to be

$$E_s^2 = E_e^2 = \frac{m_e^2 c^2 \omega_{pe}^2}{64e^2 x^4}, \quad x = \frac{V_{ph}}{V_{\text{eff}}}, \quad V_{ph} = \frac{\omega_e}{K_e}. \quad (6.10)$$

For an incident spectrum  $F_0 \propto \omega^{5/2}$ , the parameter  $x$  as determined from Equation (6.9) varies as

$$x^4(\omega_9) \simeq (x^4)_{0.1} \left(\frac{\omega_9}{0.1}\right)^{-0.22}, \quad (6.11)$$

where  $\omega_{pe} = \omega_9 \times 5 \times 10^9$  Hz. One realizes that the size of the scattering region varies with the frequency of the incident radiation. From an electron density variation of the type  $n = n_0(r/r_0)^{-\beta}$ , the size  $r$  can be expressed as a function of the plasma frequency as  $r^2 = r_0^2(\omega_9/0.01)^{-4/\beta}$  and the spectral shape of the scattered flux is given by

$$F_s = \frac{m^2 c^3}{64e^2} r_0^2 \frac{5 \times 10^9}{(x^4)_{0.1}} \left(\frac{\omega_9}{0.1}\right)^{1.22-4/\beta}. \quad (6.12)$$

Now, for radiation supported discs, Rees (1984) argues that  $\beta \sim 3$ . This gives  $\alpha \simeq -0.11$ . It is therefore distinctly possible that the radio emission typically observed with flat spectrum has a large component due to stimulated Raman scattering.

### 6.3. POLARIZATION VARIABILITY

It is well known that the Faraday effect and electron scattering can cause changes in polarization of an electromagnetic wave. In a plasma, spectral components of radiation of finite bandwidth travel different path lengths, which may lead to depolarization. Any change in the direction of the magnetic field also manifests itself through polarization variation. The strong linear polarization observed in the radio as well as in the optical regions of the spectrum in BL Lacertae objects is believed to originate in the source itself. The fact that optically violent variables and NGC 1275 show similar polarization characteristics, suggests that BL Lac objects, quasars, and Seyfert galaxies have similar sources of energy. If so, then

the lack of polarization in quasars and Seyferts would be due to depolarization effects (Stockman, 1978). The rotation of electric vector has been observed in the core-jet structure of 3C454.3 (Cotton et al., 1984) and is interpreted to be due to the propagation of radiation in a medium of varying optical thickness. Analysis of the AGN data (Aller et al., 1991) in the centimeter wavelength regime showed both flux and linear polarization variability. To explain these features, shock models with special geometries are proposed. Sillianpaa et al. (1991) observed rotation of polarization position angle linearly  $55^\circ$  in 5 hours, in OJ 287. This is the fastest ever observed position angle swing at optical wavelengths. It is difficult to explain extremely fast changes with shocks in a jet model. The SRS, being a collective process, occurs over a very short time scale and therefore is a natural candidate for affecting fast changes. The SRS of an initially elliptically polarized electromagnetic wave can be studied in the same way as for a linearly polarized wave. The electric fields of the incident  $E_i$  and the scattered  $E_s$  radiation can be written as

$$E_i = \epsilon_i [\cos(\mathbf{K}_i \cdot r - \omega_i t) \hat{e}_x + \alpha_i \cos(\mathbf{K}_i \cdot r - \omega_i t + \delta_i) \hat{e}_y],$$

$$E_s = \epsilon_s [\cos(\mathbf{K}_s \cdot r - \omega_s t) \hat{e}'_x + \alpha_s \cos(\mathbf{K}_s \cdot r - \omega_s t + \delta_s) \hat{e}'_y]$$

and the electron density variation corresponding to the electron plasma wave is expressed as

$$\delta n_e = \delta n \cos(K_e \cdot r - \omega_e t + \delta_e).$$

The coordinate system  $(\hat{e}'_x, \hat{e}'_y, \hat{e}'_z)$  is rotated through the scattering angle  $\theta_s$ , about an axis parallel to  $\hat{e}_y$ . The growth rate of the SRS instability can be determined as before except that the quiver velocity  $V_0$  is now defined as

$$\frac{V_0}{c} = \frac{e\epsilon_i \sqrt{1 + \alpha_i^2}}{m_e \omega_i c}.$$

Usually, when one talks about polarization changes, one is referring to the waves at the same frequency. SRS, however, brings about a change of frequency, but when the frequency of the incident wave is much higher than the plasma frequency, the frequency of the scattered wave differs very little from that of the incident wave. It is found that, through SRS, the clockwise-polarized radiation can change into the counter clockwise-polarized radiation and *vice versa*. In addition, the circularly polarized wave can change into a linearly polarized, a circularly polarized or an elliptically polarized wave and *vice versa*. There is also a rotation of the plane of polarization and this can take place over extremely short time scales (Gangadhara and Krishan, 1993) compared to Faraday rotation. It is shown that the incident and the Raman scattered radiation, when superimposed exhibit highly complex and variable polarization patterns, some of which could account for the observed

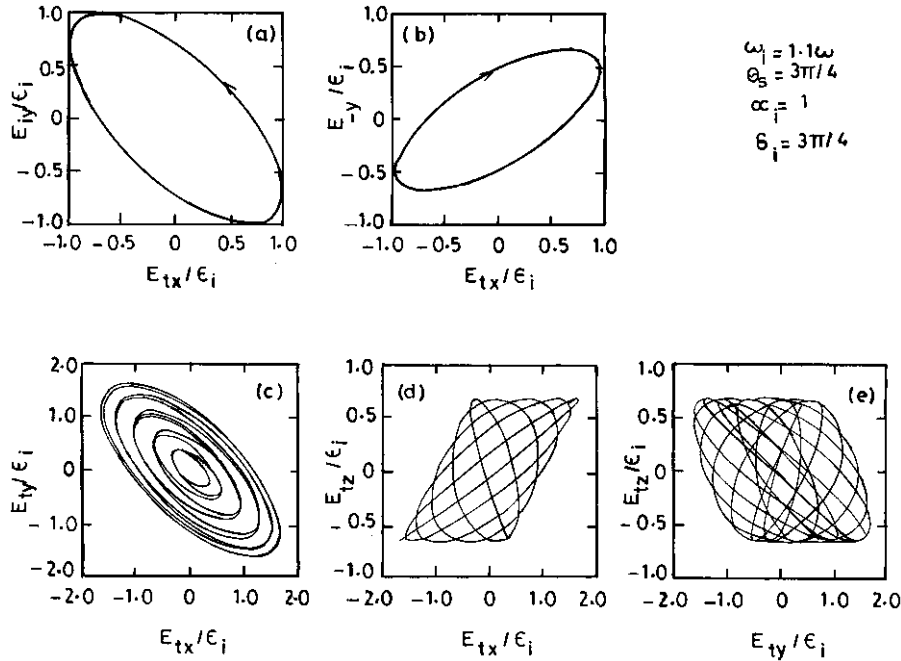


Figure 8. Parametric plots of electric fields  $E_i$ ,  $E_-$ , and  $E_t$  with respect to time  $t$ ; (a) an elliptically polarized incident wave  $E_i$  in the  $x - y$  plane; (b) the elliptically polarized scattered wave  $E_-$  in the  $x' - y'$  plane; (c) superimposed wave  $E_t$  in the  $x - y$  plane, (d) in the  $x - z$  plane; and (e) in the  $y - z$  plane.

polarization variability in intense sources. Further, if the ratio of the frequencies of the incident and the scattered radiation is an irrational number, the electric field of the superimposed radiation traces a quasi-periodic rotation. The modulation of the Raman-scattered sideband modes, with even small perturbations due to the thermal radiation or the Raman cascade, would lead to a chaotic rotation of the electric field of the superimposed radiation (Ganagadhara and Krishan, 1995). An example is shown in Figure 8.

#### 6.4. SUPERLUMINAL MOTION

The several explanations of superluminal motion include (i) a light house model in which a small change in the direction of electromagnetic beam causes a large traversal on a distant screen, exciting it in the process; (ii) relativistic beaming in which the source moving at a small angle to the line of sight with a speed slightly less than the speed of light, appears to move with superluminal speeds perpendicular to the line of sight due to light travel time effects (Blandford et al., 1977; Blandford and Konigl, 1979); (iii) gravitational lensing which can magnify the real motion and the observed flux (Barnothy, 1965). A critical discussion of these processes can be found in Scheuer (1984). The geometrical scattering of radio

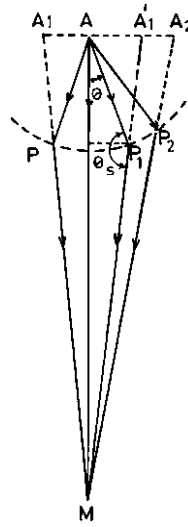


Figure 9. Apparent superluminal motion of a radio source A through geometrical scattering.

radiation can also cause superluminal expansion and or motion and halo formation. Wilson (1982) considered induced Compton scattering which, though, can give rise to light-echo effects and therefore superluminal motion but the strong frequency dependence of the motion is in contradiction with observations.

Stimulated Raman scattering can also produce the effect of superluminal motion such that the apparent motion of the source is actually the scattered radiation at increasing scattering angles. The superluminal sources generally show a core and jet configuration. The jet and features in it like knots show superluminal motion with respect to the core. In the case of radiation from a stationary source scattered by stationary plasma surrounding the source, since one does not observe a time delay between the direct and scattered paths of the radiation, the formation of virtual images for different angles of incidence results in a halo around the source. Motion may appear to take place if the source is a delta function in time and the plasma is localized along a line perpendicular to the line of sight. The apparent superluminal motion of the jet can result if source radiation beam, the fixed end of which is in the core, is rotating. Let there be a ring of plasma ( $P_1, P_2, \dots$ ) at a distance of about one parsec from the core A. The rotating radiation beam intercepts plasma at increasing angles ( $P_1, P_2, \dots$ ) as it rotates (say anticlockwise in Figure 9). To an observer at M, the Raman scattered radiation appears to come from ( $A_1, A_2, \dots$ ) corresponds to a rotation rate  $\sim 10^3$  arc sec  $\text{yr}^{-1}$  of the beam ( $AP_1, AP_2, \dots$ ). The apparent motion takes place with a uniform speed if the beam rotates at a uniform rate. The advantages of SRS over any other incoherent process are (i) the scattered radiation has an intensity almost comparable to that of the incident because under the condition  $\omega_0 \gg \omega_{pe}$ , a very small amount of energy goes to the plasma waves and thus the source does not diminish very

much as it undergoes this apparent motion and (ii) again because of  $\omega_0 \gg \omega_{pe}$ , there is no significant spectral modification of the scattered radiation, and thus the characteristics of the real source are reproduced faithfully in the virtual source generated due to SRS. Observations of the polarization differences between the core and the superluminally moving components will provide a test of this model (Krishan, 1988d).

## 7. Plasma Mechanisms for Variability

Continued studies of the rapid variability of AGN in all wave bands should prove to be extremely fruitful, as they have the potential to probe regions very close to the central engine. Processes such as refractive interstellar scintillation, gravitational microlensing, shocks propagating down jets at relativistic speeds and fluctuations in accretion disks have been considered in different sources at various spectral regions. Recent conferences on this subject include Miller and Wiita (1991) and Valtaoja and Valtonen (1992). There are several physical mechanisms dominated by plasma effects that might play a significant role in producing variability.

If accretion disks around supermassive black holes have coronae and they are permeated with structures that have transverse dimensions small compared with their lengths, like the solar coronal loops, significant density and temperature inhomogeneities are expected. These loop-like structures support a variety of magnetoacoustic oscillations with varying phase speeds consisting of sound speed, Alfvén speed and their combination. The fast and slow magnetoacoustic oscillations produce density compressions and rarefactions whereas the Alfvén wave results in only velocity variations. In AGN, the slow wave periods lie in the range of a few years and the fast mode periods are in the range of hours to months. These periods certainly do overlap with the observed microvariability time scales (Krishan and Wiita, 1994).

Continuing the solar analogy, the accretion disk loops may undergo flaring due to either anomalous Joule heating (Krishan, 1978) or due to the tearing mode instabilities. In either case, the energy stored in currents or in magnetic field configurations is released in a burst. The corresponding time scales for AGN are estimated to vary from a week to a few years (Krishan and Wiita, 1994).

An entirely separate family of instabilities arises from the interaction of electromagnetic waves with the plasma through which they propagate. These waves modify the plasma properties and in turn, the plasma acts back upon the pump wave to produce a nonlinear active medium and additional electromagnetic waves which induce temporal variability in the emerging radiation. Well-known plasma instabilities such as the Langmuir modulational instability (e.g., Zakharov, 1972), the oscillating two stream instability, and the self-modulation of electromagnetic waves in a plasma (e.g., Kaw et al., 1973) are all examples of modulational instabilities. These modulational instabilities can all be described in terms of four-

wave interactions (Gangadhara et al., 1993). These four waves consist of two pump quanta and two sidebands. The modulational instability can lead to filamentation of the wave if the modulation wavevector is perpendicular to the direction of propagation of the pump, but it can lead to a breakup of the pump beam, yielding a train of short pulses, if the modulational wavevector is parallel to the direction of propagation. Estimates in AGN show that fluctuations on subday time scales can be produced through these mechanisms (Gangadhara et al., 1993; Krishan and Wiita, 1994).

Variability could also result if there is a disruption or a change of the emission mechanism itself. The nonthermal continuum in AGN is believed to be produced by a combination of thermal, synchrotron, inverse Compton, and plasma processes. Specifically, a combination of SRS and SCS seem to account fairly well almost the entire spectrum of 3C273 (see Section 8). It is found that the change of emission process from SCS to SRS could manifest itself through a much quicker rate of energy release with a characteristic time of a few microseconds to a few milliseconds. This type of microvariability could arise if the electron beam suddenly encounters a plasma region with unfavourable parameters for one mechanism and favourable parameters for the other (Levinson and Blandford, 1995; Thompson et al., 1994; Krishan and Wiita, 1994; Coppi et al., 1993).

## 8. Nonthermal Continuum

So far, SRS and SCS in a non-relativistic plasma has been shown to account for various phenomena associated with AGN radiation. In order to investigate the role of SRS and SCS in the production of the nonthermal continuum, one has to study these processes in a relativistic plasma which is the storehouse of the energy radiated in various spectral regions. Along with the radiation processes, mechanisms for acceleration of particles should be addressed in order to ensure a steady-state emission from AGN and quasars.

A combination of stimulated Raman and Compton processes has been proposed to model the entire continuum radiation. In this picture, the gist of which was first proposed by Krishan (1983, 1985), a region of suitably varying density containing fast particles and electromagnetic fields can generate the observed continuum all the way from Radio to X-rays (and even  $\gamma$ -rays). The electrodynamic processes allow particles to be in a state of continuous acceleration as they can be accelerated by the fields they emit (Pacini and Salvati, 1982).

### 8.1. ENERGETIC ELECTRONS

The electrons are accelerated by electron-plasma waves which are produced through Raman forward-scattering (RFS). RFS is characterized by the beating of two electromagnetic waves of frequency and wave vector  $(\omega_0, \mathbf{K}_0)$  and  $(\omega_1, \mathbf{K}_1)$  respectively, so that

$$\omega_0 - \omega_1 = \omega_e \quad \text{and} \quad \mathbf{K}_0 - \mathbf{K}_1 = \mathbf{K}_e \quad (8.1)$$

and an electron plasma wave ( $\omega_e, \mathbf{K}_e$ ) is produced. The two electromagnetic waves in the context of AGN could possibly arise from cyclotron emission. For  $\omega_0 \gg \omega_{pe}$ , the phase velocity of the Langmuir waves  $V_p = \omega_e/K_e \simeq c(1 - \omega_{pe}^2/\omega_0^2)^{1/2}$  is close to  $c$ . Such a wave will grow in strength until its amplitude  $E_e$  becomes relativistic; in other words, the quiver velocity of the electrons  $V_E = eE_e/m_e\omega_e c$  approaches  $c$ . Then the wave traps electrons in the tail of the distribution and accelerates them. Because  $V_p \simeq c$ , a sizeable fraction of the electrons will stay in phase with the wave for extended periods and can thus be accelerated to high values of Lorentz factor,  $\gamma$  (Krishan and Wiita, 1990). A critical account of several popular acceleration processes in astrophysical situations is given in Colgate (1994).

## 8.2. THE SCATTERING AGENCY

The energetic electrons can radiate by being scattered in the Coulomb field of ions (Bremsstrahlung); a static magnetic field (synchrotron); a spatially periodic magnetic field, electrostatic wave and or electromagnetic wave through Raman and Compton processes. The high amplitude Langmuir waves produced by RFS may be susceptible to magnetic modulational instabilities (Beltkov and Tsytovich, 1979, 1989; Kono et al., 1981). The plasma oscillations with inhomogeneous phase distributions produce vortical currents which tend to increase the spontaneously produced magnetic fields. The magnetic modulational instability excites magnetic fields with spatial periods peaking at  $(c/\omega_{pe})$ , but ranging up to  $V_e/\omega_{pe}$  with an amplitude  $B_{MM} = eE_e^2/(4m_e c \omega_{pe})$ . This quasi-stationary spatially-periodic magnetic field will remain excited as long as the Langmuir electric field continues to be reinforced via the beating of the two electromagnetic waves. Intense localized regions of electrostatic field in the form of soliton-like structures could also provide a scattering agency (Weatherall and Benford, 1991; Lesch and Pohl, 1992). The low-frequency electromagnetic waves, say produced by the synchrotron process, could also scatter off the energetic electrons via stimulated Raman scattering in addition to the much discussed Compton scattering.

## 8.3. PRODUCTION OF RADIATION

The role of stimulated scattering process in the generation of AGN nonthermal continuum and its fast variability has been investigated since it was first pointed out (Krishan, 1983, 1985; Krishan and Wiita, 1990; Gangadhara and Krishan, 1992; Weatherall and Benford, 1991; Coppi et al., 1993; Thompson et al., 1994; Levinson and Blandford, 1995). The model consists of an electron beam which propagates radially outwards and interacts with the soft photon field to produce radiation at high frequencies. The generation (e.g., Blandford and Payne, 1982; Wiita et al., 1982) and stability of extremely sharp electron beams in quasars has been discussed by Lesch and Schlickeiser (1988). The scattering can be studied more easily in the

rest frame of the electrons, as is done in the study of inverse Compton scattering. In the rest frame of the electron beam, non-relativistic calculations of the energy transfer rates or the growth rates and the scattered flux can be carried out and these quantities can then be transferred back to the laboratory frame. In the beam frame, the beam becomes a stationary or a thermal plasma and the spatially-periodic magnetic field of period  $(k_i^{-1})$  produced by collective effects acts as an electromagnetic, wave of frequency  $\omega'_i = \gamma K_i V_b$ , the wave vector  $K'_i = \gamma K_i$  and amplitude  $E'_i = \gamma(V_b/c)B_{MM}$ , with  $V_b \simeq c$  the beam velocity. The conditions for SRS are  $\omega'_i = \omega'_s + \omega'_b$  and  $\mathbf{K}'_i = \mathbf{K}'_s + \mathbf{K}'_b$ , where  $(\omega'_s, \mathbf{K}'_s)$  and  $(\omega'_b, \mathbf{K}'_b)$  are the scattered and the electron plasma waves in the beam frame;  $\omega'_b = \omega_b = (4\pi n_b e^2/m_e)^{1/2}$  is the electron plasma frequency and  $n_b$  is the density of beam electrons. The collective nature of the scattering is lost for large  $K'_b \lambda_{De} \geq 1$  and the scattering process changes from SRS to SCS. After computing the dispersion relation in the beam frame and then transforming back into the laboratory frame, the rate of which the beam electrons lose energy via SRS is found to be (Hasegawa, 1978; Krishan, 1983):

$$\Gamma_L = \gamma^{-1} (2\beta_i^2 \omega_b^2 \gamma \omega_{pe})^{1/3}, \quad (8.2)$$

where  $\beta_i = eB_{MM}/(m\omega_{pe}c)$ , as long as  $\beta_i^2 \gg \omega_b/\gamma\omega_{pe}$ .

The density of beam electrons can be estimated by making the assumption that the rate at which beam electrons lose energy from SRS (Equation (8.2)), equals the rate at which they gain energy from RFS. Note that, while an ambient plasma has an important role in the acceleration, only the relativistic beam particles are responsible for the emitted radiation. Further, this ansatz has the pleasant consequences that a steady-state supply of relativistic electrons with small thermal spread is available.

The total power emitted by SRS can be estimated by noting that, as the scattered power rises, the effective electric field  $(\beta_i \times \mathbf{B}_s)$  produced by the scattering also increases. This field will trap the beam electrons and their thermal spread increases. The effective thermal speed is found to be

$$V_{\text{TSRS}} = \left( \frac{2e\beta_i B_s}{k'_b m_e} \right)^{1/2}, \quad (8.3)$$

where  $B_s$  is the scattered field (in the beam frame). The growth in the field is halted and the power must saturate when  $K_b = \omega_b/V_{\text{TSRS}}$ ; this is because at this point the plasma wave  $(\omega_b, K'_b)$  suffers heavy Landau damping and the radiation process shifts from SRS to SCS. Hence, the maximum value of  $B_s$  is obtained from the condition  $K'_b = (\lambda_{De})^{-1} = \omega_b/(c\Delta\gamma/\gamma)$  since  $(c\Delta\gamma/\gamma)$  is the thermal spread of the beam electrons in the beam frame. Thus, the total power emitted in the laboratory frame where the beam has velocity  $c$  is (Krishan, 1985)

$$L = \left( \frac{c}{4\pi} \right) 4B_s^2 \gamma^2 A = \left( \frac{\Delta\gamma}{\gamma} \right)^2 m c^3 \gamma^2 \beta_i^{-2} n_b A, \quad (8.4)$$

with  $A$  is the cross-sectional area of the beam (or beams). This energy is emitted essentially at the SRS scattered wave frequency

$$\omega_s = 2\gamma^2 K_{ic} = 2\gamma^2 \omega_{pe} \quad (8.5)$$

for, just as in the standard derivation of inverse Compton scattering, one power of  $\gamma$  arises in each of the Lorentz transformations into and out of the beam frame (Hasegawa, 1978). Identifying  $\omega_s$  with the maximum frequency of emission corresponding to  $K'_b \lambda_{De} = 1$ , the total power emitted at this frequency is estimated to be

$$L \sim 6 \times 10^6 n A \gamma^{-2} \xi^{-6} \text{ erg s}^{-1}, \quad (8.6)$$

where  $n$  and  $A$  are in CGS units and  $\xi^{-6}$  is a measure of the density fluctuations driven by the field  $E_e$ .

Since the frequency of emission scales with the electron plasma frequency and therefore the electron density, high frequency emission originates in the denser regions, presumably close to the very core of the AGN. It is interesting to note that the power can be made independent of frequency (corresponding to  $\alpha = 1$ , close to what is observed in the infrared X-ray region) if  $\gamma$ ,  $\xi$ , and the product  $nA$  are constants. If the beams have a constant opening angle so that  $A \propto r^2$ , then this special case corresponds to  $n \propto r^{-2}$ , the familiar law of density variation in a uniformly expanding or contracting medium. In general, assuming a power-law spatial variations of  $n$ ,  $\gamma$ ,  $\omega_s$ ,  $L(r)$ , etc., it was shown in Krishan and Wiita (1990), fairly good fits to the average AGN and Seyferts spectra could be obtained for very reasonable values of the various parameters except that electron density is taken to be higher than what is usually assumed.

The innermost regions of highest density would nominally produce extremely large amounts of optical (UV) bremsstrahlung, but because the entire plasma distribution is optically thick to such emission, very little of it escapes and the bulk of it merely serves to thermalise the plasma. The small fraction of the escaping bremsstrahlung combined with the power law emission may account for the big blue bump. This is different from the explanation given by Malkan (1983) where the big blue bump results entirely from thermal emission from an accretion disk.

One can also check that the total mass required to be in the form of a plasma, for the higher than usually considered densities, is  $\sim 10^3 - 10^4 M_\odot$  out to distances of  $10^{19}$  cm. Such values, while much greater than the mass necessarily involved in the emission line clouds (Mathews and Capriotti, 1985), are very small when compared either to the mass of the central black hole or the mass of stars expected to reside within a few parsecs of that monster; we know of no reason why they should not be acceptable.

The stimulated scattering process for the entire range of plasma and radiation parameters so as to include SRS as well as SCS and hence going through the transition region was studied by Gangadhara and Krishan (1992). Assuming a

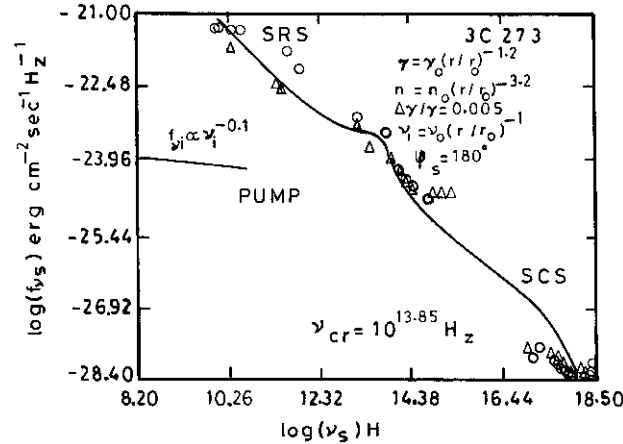


Figure 10. The spectrum of the quasar 3C273. The solid lines represent the calculated spectrum and the spectrum of the pump wave. The points represent observations (Courvoisier et al., 1987). The constants are:  $r_0 = 3 \times 10^3$ ,  $n_0 = 9.24 \times 10^{17} \text{ cm}^{-3}$ , and  $\nu_0 = 4 \times 10^{10} \text{ Hz}$ .

flat spectrum radio pump, power-law spatial variations of plasma density, Lorentz factor, temperature, and spectrum of the pump, almost the entire spectrum of 3C273 was reproduced (Figure 10). At the critical frequency ( $\nu_s \sim 10^{13.85} \text{ Hz}$ ) there is a break in the spectrum due to the change of scattering process from SRS to SCS. The SRS process contributes in the lower frequency part ( $\nu_s \leq 10^{13.85} \text{ Hz}$ ) while SCS contributes in the higher energy part. The slope of the spectrum in the SRS region is  $\sim -0.8$  and in the SCS region, it is  $(-0.7)$ . The hard X-ray part of the spectrum is steep due to strong collisional damping of the scattered and the electron plasma waves and the slope of this part is  $\sim (-1.5)$ . The bump in the spectrum is produced at the transition region ( $K_b \lambda_{De} = 0.4$ ) between SRS and SCS regions. It is clear that plasma scattering processes can contribute, in a major way, to the production of nonthermal continuum of AGN, along with its polarization and variability characteristics.

## 9. Reflections

The role of nonlinear fast plasma processes in the energetic environs of AGN and other related objects is being explored. The high brightness temperatures and rapid variability necessitate the inclusion of collective processes in the generation and propagation of electromagnetic radiation. This review, perhaps, provides only a glimpse of the yet unexplored plasma phenomena possibly occurring in high-energy sources. I believe a strong case has been made in favour of the potential carried by plasma processes in revealing the workings of intense sources like quasars and pulsars. But much remains to be done. The first thing, one should take up is to study these parametric processes in magnetized plasmas and then in inhomogeneous

plasmas. It is well known that the electric field of an electromagnetic wave swells in the resonance region ( $\omega_0 \simeq \omega_{pe}$ ) in an inhomogeneous plasma. The energy stored in this enhanced field could be tapped in the form of energetic particles and radiation. More realistic treatments of nonlinear propagation of broad band radiation needs to be performed. As these plasma processes manifest themselves in the form of instabilities, their saturation mechanisms need to be investigated in order to determine the final equilibrium. A unification of the various radiation mechanisms like Bremsstrahlung, Synchrotron, Inverse Compton and Raman scattering could be achieved if one describes these processes in terms of wave-wave scattering, since in a moving frame, the coulomb field and the magnetic field become virtual electromagnetic waves. Or perhaps there is an entirely novel way of modeling the AGN continuum. This could constitute the investigations of radiation characteristics of a turbulent plasma which is known to support a  $K^{-1}$  spectrum of electric field fluctuations ( $K$  is a wave vector). How does this translate in terms of the radiation spectrum? The field of plasma-radiation coupling is rich in scope and should be approached with an open mind towards the myriad possibilities (Krishan, 1993, 1994).

### Acknowledgements

The author is grateful to Professor P. J. Wiita of the Georgia State University (U.S.A.) and Dr Arati Chokshi of the Indian Institute of Astrophysics for critical readings of the manuscript and many useful suggestions.

### References

- Aller, M. F., Aller, H. D., and Hughes, P. A.: 1991, in J. Roland, H. Sol, and G. Pelletier (eds.), *Flux And Polarization Variability: Constraints on AGN Modeling, Extragalactic Radio Sources – From Beams to Jets, 7th IAP Meeting*, Cambridge University Press, Cambridge, p. 167.
- Antonucci, R.: 1993, 'Unified Models for Active Galactic Nuclei and Quasars', *Ann. Rev. Astron. Astrophys.* **31**, 473.
- Barnothy, J. M.: 1965, 'Quasars and the Gravitational Image Intensifier', *Astron. J.* **70**, 666.
- Barthel, P. D.: 1992, in W. J. Duschl and S. J. Wagner (eds.), *Unified Schemes for Radio-Loud and Radio-Quiet QSO's, Physics of Active Galactic Nuclei*, Springer-Verlag, Berlin, p. 637.
- Barvainis, R.: 1987, 'Hot Dust and the Near-Infrared Bump in the Continuum Spectra of Quasars and Active Galactic Nuclei', *Astrophys. J.* **320**, 537.
- Barvainis, R.: 1993, 'Free Emission and the Big Blue Bump. In Active Galactic Nuclei', *Astrophys. J.* **412**, 513.
- Belkov, S. A. and Tsyтович, V. N.: 1973, 'Modulatin Excitation of Magnetic Fields', *Soviet Phys. JETP* **49** (4), 656.
- Belkov, S. A. and Tsyтович, V. N.: 1982, 'Modulation Non-Linear Generation of the Magnetic Fields in Dense Plasma', *Phys. Scripta* **25**, 416.
- Blandford, R. D., Mckee, C. F., and Rees, M. J.: 1977, 'Super-Luminal Expansion in Extragalactic Radio Sources', *Nature* **267**, 211.
- Blandford, R. D. and Konigl, A.: 1979, 'Relativistic Jets as Compact Radio Sources', *Astrophys. J.* **232**, 34.

- Blandford, R. D. and Payne, P. G.: 1982, 'Hydromagnetic Flows from Accretion Discs and the Production of Radio Jet', *Monthly Notices Roy. Astron. Soc.* **199**, 883.
- Bregman, J. N.: 1990, *Astron. Astrophys. Rev.* **2**, 125.
- Bregman, J. N.: 1994, in T. J. L. Courvoisier and A. Blecha (eds.), 'The Origin of Continuum Emission in Active Galactic Nuclei', *IAU Symp.* **159**, 5.
- Chen, F. F.: 1974, *Introduction To Plasma Physics*, Plenum Press, London.
- Colgate, S. A.: 1994, 'Acceleration in Astrophysics', *Phys. Scripta* **T52**, 96.
- Coppi, R., Blandford, R. D., and Rees, M. J.: 1993, 'Anisotropic Induced Compton Scattering – Constraints on Models of Active Galactic Nuclei', *Monthly Notices Roy. Astron. Soc.* **262**, 603.
- Cotton, W. D. et al.: 1984, 'VLBI Observations of the Polarized Radio Emission from The Quasar 3C454.3', *Astrophys. J.* **286**, 503.
- Courvoisier, T. J. L. et al.: 1987, 'The Radio to X-Ray Continuum Emission of the Quasar 3C273 and Its Temporal Variations', *Astron. Astrophys.* **176**, 209.
- Czerny, B.: 1994, in T. J. L. Courvoisier and A. Blecha (eds.), 'Emission of Accretion Disks', *IAU Symp.* **159**, 261.
- Daltabuit, E. and Cox, D. P.: 1972, 'K Shell Photoionization Cross-Sections', *Astrophys. J.* **177**, 855.
- Daltabuit, E., MacAlpine, G. M., and Cox, D. P.: 1978, 'The Structure and Spectrum of a Colliding Cloud System and Its Possible Relationship to QSOs', *Astrophys. J.* **219**, 372.
- Davidson, K.: 1972, 'Photoionization and the Emission Line Spectra of Quasi-Stellar Objects', *Astrophys. J.* **171**, 213.
- Davidson, K. and Netzer, H.: 1979, 'The Emission Lines of Quasars and Similar Objects', *Rev. Mod. Phys.* **51**, 715.
- Edelson, R. A. and Malkan, M. A.: 1986, 'Spectral Energy Distributions of Active Galactic Nuclei Between 0.1 and 100 Microns', *Astrophys. J.* **308**, 59.
- Eilek, J. A. and Caroff, L.J.: 1976, 'Cloud Acceleration by Cosmic Rays in the Vicinity of Compact Luminous Objects', *Astrophys. J.* **208**, 887.
- Figuroa, H. et al.: 1984, 'Stimulated Raman Scattering, Two-Plasmon Decay and Hot Electron Generation from Underdense Plasma at 0.35  $\mu\text{m}$ ', *Phys. Fluids* **27**, 1887.
- Fried, D. and Conte, S. D.: 1961, 'The Plasma Dispersion Function', New York Academic, New York.
- Ginzburg, V. L. and Syrovatskii, S. I.: 1969, 'Developments in the Theory of Synchrotron Radiation and Its Reabsorption', *Ann. Rev. Astron. Astrophys.* **7**, 375.
- Gangadhara, R. T. and Krishan, V.: 1990, 'Radio Wave Heating of Astrophysical Plasmas', *J. Astrophys. Astron.* **11**, 515.
- Gangadhara, R. T. and Krishan, V.: 1992, 'The Role of Compton and Raman Scattering in the Quasar Continuum', *Monthly Notices Roy. Astron. Soc.* **256**, 111.
- Gangadhara, R. T. and Krishan, V.: 1993 'Polarization Changes of Radiation Through Stimulated Raman Scattering', *Astrophys. J.* **415**, 505.
- Gangadhara, R. T. and Krishan, V.: 1995, 'Rapid Polarization Variability in Intense Sources', *Astrophys. J.* **440**, 116.
- Gangadhara, R. T., Krishan, V., and Shukla, P. K.: 1993, 'The Modulation of Radiation in an Electron-Positron Plasma', *Monthly Notices Roy. Astron. Soc.* **262**, 151.
- Harris, E. G.: 1975, 'Introduction to Modern Theoretical Physics', Vol. 2, *Quantum Theory and Statistical Physics*, Wiley-Interscience Publ., New York, p. 735.
- Hasegawa, A.: 1978, 'Free Electron Laser', *Bell System Tech. J.* **57**, 3069.
- Hoyle, F., Burbidge, G. R., and Sargent, W. L. W.: 1966, 'On the Nature of the Quasi-Stellar Sources', *Nature* **209**, 751.
- Hughes, P. A., Aller, H. D., and Aller, M. F.: 1985, 'Polarized Radio Outburst in BL LACERTEA II: The Flux And Polarization of A Piston-Driven Shock', *Astrophys. J.* **298**, 301.
- Jones, T. W., O'Dell, S. L., and Stein, W. A.: 1974, 'Physics of Compact Non-Thermal Sources II: Determination of Physical Parameters', *Astrophys. J.* **192**, 261.
- Kaw, P. K., Schmidt, G., and Wilcox, T.: 1973, 'Filamentation and Trapping of Electromagnetic Radiation in Plasmas', *Phys. Fluids* **16**, 1522.
- Kniffen, D. A. et al.: 'Time Variability in the Gamma-Ray Emission of 3C279', *Astrophys. J.* **411**, 133.

- Kono, M., Skoric, M. M., and ter Haar, D.: 1981, 'Spontaneous Excitation of Magnetic Fields and Collapse Dynamics in a Langmuir Plasma', *J. Plasma Phys.* **26**, 123.
- Krishan, V.: 1978, 'Conductivity of an Ion-Acoustically Turbulent Plasma', *Solar Phys.* **59**, 29.
- Krishan, V.: 1983, 'Emission Mechanism of Extragalactic X-ray and Radio Sources', *Astrophys. Lett.* **23**, 133.
- Krishan, V.: 1985, 'Acceleration and Radiation Processes Around Active Galactic Nuclei', *Astrophys. Space Sci.* **115**, 119.
- Krishan, V.: 1987, 'Anomalous Heating of Quasar Emission – Line Regions', *Monthly Notices Roy. Astron. Soc.* **226**, 629.
- Krishan, V.: 1988a, 'Is 21-cm Absorption Associated with the Emission-Line Regions of Quasars', *Monthly Notices Roy. Astron. Soc.* **231**, 357.
- Krishan, V.: 1988b, 'Scattering of Quasar Radiation in the Intercloud Medium', *Monthly Notices Roy. Astron. Soc.* **234**, 79.
- Krishan, V.: 1988c, 'Raman Scattering of the Synchrotron Self-Absorbed Radiation in Accretion Discs', *Monthly Notices Roy. Astron. Soc.* **230**, 183.
- Krishan, V.: 1988d, 'One More Explanation of Superluminal Motion', *J. Astrophys. Astron.* **9**, 231.
- Krishan, V.: 1993, 'The Extraterrestrial Raman Scattering', *Current Sci.* **64**, 301.
- Krishan, V.: 1994, 'Role of Plasma Processes in Astrophysics', *Phys. Scripta* **T52**, 118.
- Krishan, V. and Wiita, P. J.: 1990, 'Coherent Plasma Processes and the Continuum Emission in Active Galactic Nuclei', *Monthly Notices Roy. Astron. Soc.* **246**, 597.
- Krishan, V. and Wiita, P. J.: 1994, 'Plasma Mechanisms for Variability in Active Galactic Nuclei', *Astrophys. J.* **423**, 172.
- Krolik, J. H., McKee, C. F., and Tarter, C. B.: 1978, in A. Wolfe (ed.), *Proc. Pittsburgh Conference on BL Lacertae Objects*, University of Pittsburgh, Pittsburgh, p. 277.
- Krolik, J. H., McKee, C. F., and Tarter, C. B.: 1981, 'Quasar Emission Line Regions', *Astrophys. J.* **249**, 492.
- Kruer, L. W.: 1988, *The Physics of Laser Plasma Interactions*, Addison-Wesley Publ. Co. Inc., New York.
- Lesch, H. and Pohl, M.: 1992, 'A Possible Explanation for Intraday Variability in Active Galactic Nuclei, Magnetic Reconnection And Coherent Plasma Emission', *Astron. Astrophys.* **254**, 29.
- Lesch, H. and Schlickeiser, R.: 1987, 'Stabilization and Consequences of Relativistic Electron Bumps in Extragalactic Radio Sources', *Astron. Astrophys.* **179**, 93.
- Levich, E. V. and Sunyaev, R. A.: 1971, 'Heating of Gas near Quasars, Seyfert-Galaxy Nuclei and Pulsars by Low-Frequency Radiation', *Soviet Astron.* **15**, 363.
- Levinson, A. and Blandford, R.: 1995, 'Raman Scattering in High-Radio-Brightness Astrophysical Systems: Application to Active Galactic Nuclei', *Monthly Notices Roy. Astron. Soc.* **274**, 717.
- Lightman, A. P.: 1982, 'Relativistic Thermal Plasma: Pair Processes and Equilibria', *Astrophys. J.* **253**, 849.
- Liu, C. S. and Kaw, P.: 1976, 'Parametric Instabilities in Homogeneous Unmagnetized Plasmas', *Adv. Plasma Phys.* **6**, 83.
- Malkan, M. A.: 1991, in C. Bertout, S. Collin, J. P. Lasota, and J. Tran Thanh Van (eds.), 'Accretion Disk Models for Active Galactic Nuclei', *Structure and Emission Properties of Accretion Disks*, Ed. Frontiers, Gif-sur-Yvette, p. 165.
- Malkan, M. A.: 1992, in W. J. Duschl and S. J. Wagner (eds.), 'Examining Alternatives to Accretion Disk Models for the AGN Continuum', *Physics of Active Galactic Nuclei*, Springer-Verlag, Berlin, p. 109.
- Mannheim, K.: 1994, T. J. L. Courvoisier and A. Blecha (eds.), *On the Difference Between Radio Loud and Radio Quiet AGN, Multiwavelength Continuum Emission of AGN*, Kluwer Academic Publishers, Dordrecht, p. 285.
- Marscher, A. P. and Bloom, S. D.: 1992, *Compton Observatory Science Workshop*, p. 346.
- McCray, R.: 1979, in C. Hazard and S. Mitton (eds.), 'Spherical Accretion onto Supermassive Black Holes', *Active Galactic Nuclei*, Proceedings of a Nato Study Institute held at the Institute of Astronomy, University of Cambridge, Cambridge, p. 227.

- Mathews, W. G. and Capiotti, E. R.: 1985, in J. S. Miller (ed.), 'Structure and Dynamics of the Broad Line Regions', *Astrophysics of Active Galaxies and Quasi-Stellar Objects*, University Science Books, Mill Valley, p. 185.
- Miller, H. R. and Wiita, P. J. (eds.): 1991, *Variability of Active Galactic Nuclei*, Cambridge University Press, Cambridge.
- Mushotzky, R. F., Done, C., and Pounds, K. A.: 1993, 'X-Ray Spectra and Time Variability of Active Galactic Nuclei', *Ann. Rev. Astron. Astrophys.* **31**, 13.
- Novikov, I. and Thorne, K. S.: 1973, in C. Dewitt and B. Dewitt (eds.), 'Black Hole Astrophysics' *Black Holes*, Gordon and Breach, New York, p. 343.
- Nussbaumer, H. and Osterbrock, D. E.: 1970, 'On the Forbidden Emission Lines of Iron in Seyfert Galaxies', *Astrophys. J.* **161**, 811.
- Osterbrock, D. E. and Mathews, W. G.: 1986, 'X-Ray Spectra and Time Variability of Active Galactic Nuclei', *Ann. Rev. Astron. Astrophys.* **31**, 717.
- Osterbrock, D. E. and Parker, R. A. R.: 1965, 'Physical Conditions in the Nucleus of the Seyfert Galaxy NGC 1068', *Astrophys. J.* **141**, 892.
- Pacholczyk, A. G.: 1970, *Radio Astrophysics*, Freeman, San Francisco.
- Pacini, F. and Salvati, F.: 1982, in D. S. Heesch and C. M. Wade (eds.), 'The Nature of the Energy Source in Radio Galaxies and Active Galactic Nuclei, Extragalactic Radio Sources', *IAU Symp.* **97**, 247.
- Phinney, E. S.: 1985, J. S. Miller (ed.), 'Central Radio Sources', *Astrophysics of Active Galaxies and Quasi-Stellar Objects*, Oxford University Press, Oxford, p. 453.
- Rees, M. J.: 1966 'Appearance of Relativistically Expanding Radio Sources', *Nature*, **211**, 468.
- Rees, M. J.: 1977, 'Quasar Theories', *Ann. N.Y. Acad. Sci.* **302**, 613.
- Rees, M. J.: 1984, 'Black Hole Models for Active Galactic Nuclei', *Ann. Rev. Astron. Astrophys.* **22**, 471.
- Rees, M. J. et al.: 1969, 'Infrared Radiation from Dust in Seyfert Galaxies', *Nature* **223**, 788.
- Rieke, G. H.: 1978, 'The Infrared Emission of Seyfert Galaxies', *Astrophys. J.* **226**, 550.
- Robson, E. I. et al.: 1986, 'A New Infrared Spectral Component of the Quasar 3C273', *Nature* **323**, 134.
- Rybicki, G. B. and Lightman, A. P.: 1979, *Radiative Processes in Astrophysics*, Wiley-Interscience Publication, New York.
- Scheuer, P. A. G.: 1984, in R. Fanti, K. Kellermann and G. Setti (eds.), 'Explanations of Superluminal Motion', *IAU Symp.* **110**, 197.
- Scheuer, P. A. G.: 1995, 'Lobe Asymmetry and the Expansion Speeds of Radio Sources', *Monthly Notices Roy. Astron. Soc.* **277**, 331.
- Shields, G. A.: 1978, 'Thermal Continuum from Accretion Disks in Quasars', *Nature* **272**, 706.
- Sillanpaa, A., Nilsson, K., and Takalo, L. O.: 1991, in J. Roland, H. Sol, and G. Pelletier (eds.), 'Rapid 55 Degree Swing in the Position Angle of the Polarization in OJ 287: A Flare in the Accretion Disk?', *Extragalactic Radio Sources - From Beams to Jets, 7th IAP Meeting*, Cambridge University Press, Cambridge, p. 174.
- Spangler, S. R.: 1982, in D. S. Heesch and C. M. Wade (eds.), 'Spectral Shapes of Compact Extragalactic Radio Sources', *Extragalactic Radio Sources*, D. Reidel Publ. Co., Dordrecht, Holland, p. 297.
- Stein, W. A. and O'Dell, S. A.: 1985, in J. S. Miller (ed.), 'The Radio to X-Ray Continua of AGN', *Astrophysics of Active Galaxies and Quasi-Stellar Objects*, Oxford University Press, Oxford, p. 381.
- Stockman, H. S.: 1978, in A.-M. Wolfe (ed.), 'A Report on the Liner Polarization Survey' *Pittsburgh Conference on BL Lac Objects*, University of Pittsburgh, Pittsburgh, p. 149.
- Svensson, R.: 1982, 'Electron-Positron Pair Equilibria in Relativistic Plasmas', *Astrophys. J.* **258**, 335.
- Svensson, R.: 1984, 'Steady Mildly Relativistic Thermal Plasma: Processes and Properties', *Monthly Notices Roy. Astron. Soc.* **209**, 175.
- Tamor, S.: 1973, 'Effect of Partial Coherence on Laser-Driven Plasma Instabilities', *Phys. Fluids* **16**, 1169.

- Thomson, J. J. et al.: 1974, 'Parametric Instability Thresholds and Their Control', *Phys. Fluids* **17**, 849.
- Urry, C. M. and Padovani, P.: 1995, *Publ. Astron. Soc. Pacific* **107**, 803.
- Valtaoja, E. and Valtonen, M.: 1992, *Variability of Blazars*, Cambridge University Press, Cambridge.
- Weatherall, J. C. and Benford, G.: 1991, 'Coherent Radiation from Energetic Electron Streams via Collisionless Bremsstrahlung in Strong Plasma Turbulence', *Astrophys. J.* **378**, 543.
- Weymann, R. J., Carswell, R. F., and Smith, M. G.: 1981, 'Absorption Lines in the Spectra of Quasistellar Objects', *Ann. Rev. Astron. Astrophys.* **19**, 41.
- Wiita, P. J., Kapahi, V. K., and Saikia, D. J.: 1982, 'Relativistic Beams, Thick Accretion Disks and Active Galactic Nuclei', *Bull. Astron. Soc. India* **10**, 310.
- Wilson, D. B.: 1982, 'Induced Compton Scattering in Radiative Transfer', *Monthly Notices Roy. Astron. Soc.* **200**, 881.
- Wilson, A. S. and Colbert, E. J. M.: 1995, 'The Difference Between Radio-Loud and Radio-Quiet Active Galaxies', *Astrophys. J.* **438**, 62.
- Zakharov, V. E.: 1972, 'Collapse of Langmuir Waves', *Soviet Phys. – JETP* **35**, 908.
- Zdziarski, A. A. et al.: 1990, 'Electron-Positron Pairs, Compton Reflection and the X-Ray Spectra of Active Galactic Nuclei', *Astrophys. J.* **363**, L1.